UC Davis

UC Davis Previously Published Works

Title

Reenvisioning cross-sectional at-a-station hydraulic geometry as spatially explicit hydraulic topography

Permalink

https://escholarship.org/uc/item/4453s7r0

Journal

Geomorphology, 246

ISSN

0169555X

Authors

Gonzalez, R.L.
Pasternack, G.B.

Publication Date

2015-10-01

DOI

10.1016/j.geomorph.2015.06.024

Peer reviewed

eScholarship.org Powered by the California Digital Library
University of California

Reenvisioning cross-sectional at-a-station hydraulic geometry as spatially explicit hydraulic topography

R.L. Gonzalez* and G.B. Pasternack

University of California, Davis, One Shields Drive, Davis, CA 95616, USA

*Corresponding author Tel.: + 1 619-379-5375.

E-mail: robgonzalez@ucdavis.edu.

UNCORRECTED FINAL MANUSCRIPT

Abstract

Transect-based hydraulic geometry is well established but depends on a complex set of subjective fieldwork and computational decisions that sometimes go unexplained. As a result, it is ripe for reenvisioning in light of the emergence of meter-scale, spatially explicit data and algorithmic geospatial analysis. This study developed and evaluated a new spatially explicit method for analyzing discharge-dependent hydraulics coined 'hydraulic topography' that not only increases accuracy but also eliminates several sample- and assumption-based inconsistencies. Using data and hydrodynamic simulations from the regulated, gravel-cobble-bed lower Yuba River in California, power functions were fitted to discharge-dependent average width, depth, and depth-weighted velocity for three spatial scales and then their corresponding exponents and coefficients were compared across scales and against ones computed using traditional approaches. Average hydraulic values from cross sections at the segment scale spanned up to 1.5 orders of magnitude for a given discharge. Transect-determined exponents for reach-scale depth and velocity relations were consistently over- and underestimated, respectively, relative to the hydraulic topography benchmark. Overall, 73% of cross-sectional power regression parameters assessed fell between 10 and 50 absolute percent error with respect to the spatially explicit hydraulic topography baseline. Although traditional transect-based sampling may be viable for certain uses, percent errors of this magnitude could compromise engineering applications in river management and training works.

Keywords: hydraulic geometry; river modeling; gravel-bed rivers; fluvial geomorphology

UNCORRECTED FINAL MANUSCRIPT

1. Introduction

The use of hydraulic geometry (HG) relations is widespread in river science and restoration. At-a-station HG relationships have been applied in geomorphic process assessment (Knighton, 1975; Merigliano, 1997; Pasternack, 2011), river restoration (Copeland et al., 2001; Shields et al., 2003), stream classification (Leopold and Wolman, 1957; Rosgen, 1994), waterfall systematics (Wyrick and Pasternack, 2008), aquatic ecosystem evaluation (Hogan and Church, 1989; Jowett, 1998), and estimating river discharge from satellites (Gleason and Smith, 2014). However, sampling bias and differences in post-processing create inconsistencies across HG studies that can make comparisons difficult. Additionally, recognizing and accounting for the effects of geometric channel variability and complexity has generally been omitted from traditional HG sampling such that the resulting HG exponents and coefficients may not adequately represent the range of channel hydraulics.

Current technology allows for meter-scale topographic mapping (e.g., Brasington et al., 2000; Hilldale and Raff, 2007; Williams et al., 2014) and multidimensional hydrodynamic modeling (e.g., Horritt and Bates, 2002; Zhang and Shen, 2008) of rivers, yielding sufficient data for a novel, alternative approach that could comprehensively represent the state of a river without all the problems caused by estimation through sampling. The term ‘near-census’ is used herein to refer to comprehensive, spatially explicit, process-based approaches using the 1-m scale as the basic building block for investigating rivers in light of the emerging abundance of meter-scale topographic data sets without the confounding problems associated with sampling. The concept of a ‘near-census’ implies that meter-scale data represents variables in great detail that

UNCORRECTED FINAL MANUSCRIPT

approaches the population of conditions, but that there remains a finer level of detail in the domain of continuum mechanics that eventually will be resolved with further technological developments. For example, decimeter-scale terrain variability captured using airborne terrestrial LiDAR has been shown to contain hydraulically relevant information in urban settings (Sampson et al., 2012; Ozdemir et al., 2013). The overall goal of this study was to present such a new approach (termed 'hydraulic topography' (HT) to differentiate it from conventional cross section HG relations), report the results of applying it to a sizable river segment, and then evaluate differences between HG and HT analyses. In addition, this study tested key traditional HG sampling methods to show significant uncertainties in contrast to common perceptions.

1.1. At-a-station hydraulic geometry basics

Hydraulic geometry relations are power functions relating wetted channel width (W), mean flow depth (D), and mean velocity (V) to discharge (Q):

$$W = aQ^b \quad D = cQ^f \quad V = kQ^m \qquad (1) – (3)$$

where a, c, k, b, f, and m are parameters (Leopold and Maddock, 1953). When constructed for changes in discharge over time at one cross section, Eqs. (1–3) address how channel geometry accommodates changing discharge. Beginning with a triangular channel cross section, changing exponents of Eqs. (1) and (2) bends cross-sectional shape, while changing coefficients stretches it (Wyrick and Pasternack, 2008). Continuity requires that $a \cdot c \cdot k$ and $b+f+m$ both equal unity at a channel cross section, but

UNCORRECTED FINAL MANUSCRIPT

not when derived from multiple transects with different shapes.

The idea that the HG of long river domains of varying depth and width can be reasonably represented with limited cross-sectional data is prevalent (Wolman and Brush, 1961; Langbein, 1964; Stewardson, 2005). Yet, it is also acknowledged that the mean state of a river is difficult to determine because of high variability between cross sections (Knighton, 1975; Rhodes, 1977). Differences in at-a-station HG have been observed between riffles and pools (Knighton, 1975, 1998), braided and nonbraided rivers (Knighton, 1974; Rhodes, 1977), and on the basis of variable bed substrate (Williams, 1978; Xu, 2004), bank vegetation (Andrews, 1984), and bank cohesion (Knighton, 1974).

1.2. Uncertainties in at-a-station hydraulic geometry

Despite extensive use of HG, few studies address the assumptions or explain the procedural steps in sufficient detail for repeatability. Sampling, as a paradigm for hypothesis testing in the scientific method, is inherently biased and fraught with confounding complexities relating to study-specific choices, many of which may go unexplained or unsupported in the literature for many reasons (Fig. 1). A detailed explanation is presented in the supplemental materials, section 1.2. A complex array of interdependent factors influence HG relations, yet authors commonly assume HG exponents are acceptable because they fall within the range of globally (Jowett, 1998) or regionally (Andrews, 1984) reported values. Studies from around the world yielded ranges for at-a-station HG exponents *b*, *f*, and *m* of 0.0–0.59, 0.06–0.73, and 0.07–0.71, respectively; from the same at-a-station data set (n = 139), the modal class for *b*, *f*, and

UNCORRECTED FINAL MANUSCRIPT

m was 0.0–0.1, 0.3–0.4, and 0.4–0.5, respectively (Park, 1977). Several study comparisons discuss the variation between HG exponents (Knighton, 1975; Park, 1977; Singh, 2003; Xu, 2004) but offer little explanation of the limitations associated with those data sources or their comparability. Based on the lack of HG details and the frequency of cross-study HG comparisons, one may conclude that geomorphologists assume the methodology is consistent. Knighton (1975) suggested a systematic selection of stable cross sections based on similar geometry and bank material to reduce variability. However, if the goal is to characterize rivers as they actually exist, including the full range of natural variability, then it is important to sample traditionally avoided transects.

1.3. Spatial scale challenges

Characterizing HG with transect sampling strategies is challenging because attributes and metrics vary with spatial scale. Herein, spatial scales are defined as segment (~ 10^3–10^4 *W*), reach (~ 10^2–10^3 *W*), and morphological unit (~ 10^0–10^1 *W*). At the segment scale, Pitlick and Cress (2002) sampled cross sections every 1.6 km along 260 km of the Colorado River. At the reach scale, two approaches commonly used have been (i) sampling in proportion to the abundance of morphological units (Rosgen and Silvey, 1996) and (ii) weighting by the distance between cross sections (Jowett, 1998; Stewardson, 2005; Navratil and Albert, 2010). According to Navratil and Albert (2010), major uncertainties associated with characterizing larger sections of river are related to river choice, its length, the number of cross sections surveyed, and the range of flows considered. At the morphological unit scale, single cross sections have been used when analyzing pool and riffles (Richards, 1976a, b).

UNCORRECTED FINAL MANUSCRIPT

1.4. Hydraulic modeling to study hydraulic geometry

Hydraulic geometry source data can be obtained theoretically, empirically, or numerically. Empirical approaches rely on extensive field measurements at many sites, each for a range of discharges. Numerical modeling requires topographic data, a stage-discharge relation for the model terminus, and parameter values. One-dimensional (1D) hydrodynamic modeling has been used to derive HG relations (Brown and Pasternack, 2008; Navratil and Albert, 2010). However, Navratil and Albert (2010) postulated that 2D models are better to understand linkages between vegetation, sediment size, and reach-scale hydraulic properties. Only Sawyer et al. (2010) performed HG analyses using 2D modeling and inclusion of hydraulic roughness elements associated with spatially explicit vegetation patches. Three-dimensional models could be used to simulate river hydraulics and then averaged vertically.

1.5. Research objectives

This study introduces and assesses a new near-census approach called hydraulic topography, which was inspired by at-a-station HG analysis. Near-census data enables averaging at each spatial scale to yield HT relations that account for the full range of data variability at the 1-m scale, which should be of greater scientific and management value. This also minimizes uncertainty in multiscalar river attributes caused by inadequate sampling, interpolations, and extrapolations. The specific study objectives were to (i) determine how HT regression curves, exponents, and coefficients compare to corresponding HG results at segment, reach, and morphological unit spatial

UNCORRECTED FINAL MANUSCRIPT

scales with two different sampling densities; (ii) characterize the spread in traditional HG exponents and coefficients for each scale; and (iii) test diverse aspects of traditional HG sampling methods.

With regard to the third objective, multiple tests were done, but for brevity only two are presented herein given their significance for understanding the suitability of sampling as a paradigm for river science and management. First, does increasing transect sample density over a common amount of sampling by a factor of 10 improve results in terms of more closely matching the HT of the population of conditions? The classic expectation is that a reasonable amount of sampling, such as a low double-digit number of cross sections, would do well at characterizing a unit; but this expectation has not been tested among different numbers of cross sections, let alone comparing between HG and HT approaches. Further, classic expectation posits that accuracy will improve with increased sampling. Whether such improvement would occur at a linear, exponential, or other rate is also in question. Second, is there a representative station for each unit at each scale in the sense that it shares the same numerical values as the HT average of the unit? The classic expectation is that individual cross sections represent units at each scale and that experts are able to go find and use them for low-cost small sampling instead of doing a census. The results from this study are able to answer these important questions and evaluate commonly held assumptions of traditional methodology, which is a significant advancement to aid fluvial geomorphology.

UNCORRECTED FINAL MANUSCRIPT

2. Study site

This study used data and models from the gravel-cobble–bedded lower Yuba River (LYR) within the 3480-km^2 Yuba River catchment in north-central California, USA (Fig. 2). This river segment spans ~ 37.4 km from Englebright Dam to the confluence with the Feather River. Dam outlets may only regulate flows < 90% of bankfull discharge. Pasternack (2010) summarized the existing information about LYR hydrology, hydraulics, and geomorphology with subsequent additions including Carley et al. (2012), Abu-Aly et al. (2013), and Wyrick and Pasternack (2014).

The LYR segment was delineated into eight distinct geomorphic reaches based on physical variables that govern sediment transport capacity, sediment supply, and topography (Wyrick and Pasternack, 2012). The underlying variables of discharge from mainstem-tributary confluences, man-made structures, valley width, bed slope, and bed material type were all used to define reach breaks along the LYR. The geomorphic reaches analyzed in this study were chosen to maximize differences to gain diversity in HG relations (Table 1; Fig. 2). Timbuctoo Bend has a valley-constrained, single-threaded, slightly sinuous channel in a valley bend. It has central bars and riffle crests alternating longitudinally with pools located at dominant bedrock constrictions that are thought to control morphodynamics (White et al., 2010). Daguerre Point dam (DPD) is a low-height concrete barrier. The DPD reach starts below the dam and ends at a distinct slope break 5639 m downstream. It has an actively meandering channel with a substantially wider mean bankfull width compared to the other reaches and a parallel overflow side channel. Its channel is partially constrained by artificial alluvial berms. The Marysville reach is the lowermost 5334 m ending at the confluence with the Feather

UNCORRECTED FINAL MANUSCRIPT

River. It has a nearly trapezoidal straight alluvial channel confined laterally by flood control levees.

In the past, morphological unit (MU) delineation has been mostly qualitative in nature and focused on differentiating between riffles and pools, thus there are many working definitions (Wadeson, 1994). Recently, however, an objective and discharge-independent method that classifies channel hydraulics into a suite of MUs was developed and implemented on the LYR (Wyrick and Pasternack, 2014). A pool was conceived to be a topographic low in the channel that exhibits relatively high depth, low velocity, and low surface water slope at a representative base flow (~ 15% of bankfull discharge) ideal for revealing underlying topographic patterns and then mapped using 2D model simulations. This concept was turned into a specific joint range of depth (> 1.4 m) and velocity (< 0.6 m/s) for the representative base flow. A riffle was conceived as a shallow area with moderate to high velocities, rough water surface texture, and steep water surface slope at the same representative base flow. The hydraulic thresholds for riffle on the LYR at the representative base flow were meter-scale depths < 0.7 m and velocities > 0.6 m/s. Near-census MU analysis of the LYR revealed 328,914 m^2 of pool and 272,282 m^2 of riffle. Six other in-channel bed landforms were delineated with other ranges of depth and velocity but were not used in this study given a lack of preexisting at-a-station HG studies of MUs other than pools and riffles. The resulting map of spatially explicit polygons of each MU type was proven to not be sensitive to the exact base-flow discharge value within a range of up to 20% of the preferred value chosen. These hydraulic riffle and pool delineations from Wyrick and Pasternack (2014) are the basis for HG analyses at the MU scale in this study.

UNCORRECTED FINAL MANUSCRIPT

222

223 **3. Methods**

224 This section briefly describes the spatially explicit data used in the study, data
225 processing to obtain HT and HG results, and data analysis procedures addressing study
226 objectives. Full underpinnings of the data, 2D models and their validation, and specific
227 HT and HG processing steps are explained in the supplementary materials (section 3).
228 Data in this study were collected and generated in English units consistent with
229 regulatory requirements (Pasternack, 2009) and then converted to SI units, hence the
230 appearance of noninteger lengths, areas, and volumes below.

231 To develop the HT approach and use it to evaluate uncertainty in at-a-station HG
232 analysis, this study relied on testbed near-census topographic data and 2D
233 hydrodynamic models developed and validated as part of the LYR management
234 program (YARMT, 2010). The testbed was a real river as opposed to a synthetic river
235 (e.g., Brown and Pasternack, 2009) to have multiple scales of natural landform
236 variability. Hydrodynamic simulations predicted depth and depth-averaged velocities
237 throughout ~ 37 river km for discharges ranging from 0.2 to 20 times bankfull (8.495–
238 2831.7 m^3/s) (Barker, 2011; Abu-Aly et al., 2013; Pasternack et al., 2014). The study
239 herein only used the 20 simulations up to bankfull discharge (141.584 m^3/s). Model
240 results were used to produce 0.9144-m resolution depth and velocity rasters.

241

242 *3.1. Hydraulic topography analysis*

243 The new HT analysis represents discharge-dependent, spatially averaged river
244 hydraulics without many of the HG problems illustrated in Fig. 1. Unlike traditional

UNCORRECTED FINAL MANUSCRIPT

methods for determining HG, HT relies on 2D hydrodynamic simulations founded on thorough (meter-scale) and thoughtful topographic and bathymetric mapping of the entire river segment, not just at a select number of transects. In the future, 3D hydrodynamic modeling or meter-scale remote sensing of depth and velocity could be used instead. Although hydraulic topography introduces some new decisions regarding which model to use and how, it substantially diminishes the bias associated with common field data collection. Also, whereas field methods involve irreversible and unreported decisions made in the field, modeling and geospatial analysis allow for transparent workflows and algorithms that can be revised and rerun at any stage of production and review.

To obtain HT metrics, depth rasters were spatially averaged in ArcGIS at each discharge for every spatial scale using the Spatial Analyst tool called 'Zone Statistics as Table'. Velocity rasters were handled somewhat differently, as they represented depth-averaged velocity magnitudes. To apply the same spatial averaging treatment would have weighted shallow, slow-moving and deep, fast-moving cells equally. Even though that is valid data, to make the analysis comparable to the standard HG approach, it was necessary to first depth-weight velocities. To do this, mean velocities were determined at each scale by first multiplying individual velocity cell values by the ratio of cell depth to the average depth within the sampling domain at the relevant scale (i.e., the whole segment, within only a specified reach, or within only a specified MU type) for a given discharge. The resulting velocity raster was 'weighted by depth' and then averaged over the same spatial scale using the 'Zone Statistics as Table' tool. This calculation was done for all 20 discharges and each spatial scale combination. Near-census mean

UNCORRECTED FINAL MANUSCRIPT

values of depth and depth-weighted velocity were plotted as a function of discharge and fitted with power functions (Eqs. 1–3). The coefficients and exponents of the power functions were identified.

Segment and reach near-census width analyses relied on cross sections spaced uniformly every 6.096 m (~ 1/16 of mean bankfull channel width) along and perpendicular to the LYR valley centerline. Though arbitrary, this choice yielded data sufficiently dense to be considered near-census for the population of width values. Cross-sectional wetted widths were computed along the entire segment and tabulated for each flow in ArcGIS. Because near-census MUs are arbitrarily shaped landforms that do not span the channel, HT width analysis was not done at the MU scale. The geometric means of channel widths were calculated for the segment and each reach at each discharge, then plotted and fitted with power functions. The coefficients and exponents of the power functions were identified.

3.2. Hydraulic geometry analysis

3.2.1. Cross-sectional sampling

Depth and velocity rasters were sampled and analyzed for at-a-station hydraulic geometry relations at segment, reach, and MU spatial scales. Segment and reach cross-sectional analyses were based on ~ 100-m (97.54 m) and ~ 1-km (975.4 m) longitudinally spaced subsets of the uniformly spaced cross section set used to obtain channel width for the near-census representation. The number of cross sections used per sample method is listed for each spatial scale in Table 2. At the segment scale, the use of 36 and 354 cross sections represent, respectively, the typical small sampling

UNCORRECTED FINAL MANUSCRIPT

commonly done in practice and an extremely heroic field effort. Neither hundreds of cross sections nor 20 discharges up to bankfull are surveyed for HG relations, but these amounts were used to represent the maximum likely effort. This allowed for tests of whether even such an extreme effort of sampling improves results over the typical smaller sampling relative to HT results.

Morphological units were sampled using a consistent, traditional geomorphic approach and focusing on riffles and pools as traditionally done. Riffles and pools were selected among those with an area > 92.8 m^2 (≥ 111 pixels) to have landforms with a length scale of > 0.3 W — 95% and 98% of total riffle and pool area, respectively. Regions likely to be avoided in fieldwork were further excluded: highly oblique landforms, areas of channel braiding, and regions with large backwater extents — this was done to ensure the MU was a dominant station feature. Individual units were randomly selected among those that met the above MU sampling criteria. Cross sections were placed at the visual center of each MU normal to the valley centerline. Width, depth, and velocity data at each MU cross section were aggregated the same as for cross-sectional reach scale. In all, 15 riffles and 14 pools were analyzed by cross section as such numbers might be feasibly measured during a field campaign.

3.2.2. Hydraulic geometry computations

Width, depth, and velocity HG relations were produced as similarly as possible, but each data type required some unique steps. Width was the simplest mean hydraulic variable to calculate because there was only one value to consider for each cross section at each flow for each spatial scale. The geometric mean was computed using all

UNCORRECTED FINAL MANUSCRIPT

cross-sectional widths that fell within the scale of interest, and that was repeated for each flow to develop a width-discharge relationship curve. Depth was sampled at 30 evenly spaced points along each wetted cross section and then arithmetically averaged to a single value for each cross section before the geometric mean was computed for the set of cross sections for each flow (Turnipseed and Sauer, 2010). Velocity calculations involved 'depth weighting' per standard HG procedure. First, each of the thirty velocity sample points along a cross section was multiplied by the ratio of local to average cross-sectional depth. Results were then arithmetically averaged along each cross section before computing the geometric mean among all cross sections for each flow. Power functions (Eqs. 1–3) were fitted to mean width, depth, and depth-weighted velocity for each discharge at each spatial scale; and the coefficients and exponents were computed. At segment and reach scales, this was done independently for the 100-m and 1-km data sets.

3.3. Data analyses

To address the research objectives, four different data analyses were undertaken, each with multiple evaluation metrics. First, trend functions in stacked log-linear regressions of HT and HG variables versus discharge were visually compared to help uncover systematic variations between the hydraulics for each method. The HT and HG power functions and their parameters were inspected and compared at each spatial scale. Key evaluation metrics included (i) the mean power functions themselves, (ii) the range of cross-sectionally averaged HG data for the 100-m sampling set, (iii) ternary and binary plots of the power function exponents, and (iv) percent differences

UNCORRECTED FINAL MANUSCRIPT

for exponents and coefficients of fitted power functions between each HG analysis and its corresponding HT baseline. Performance thresholds for error percent were transparently defined on an expert basis to help interpret the sampling results. If percent error magnitude was ≤ 10, then transect performance was deemed good. If percent error magnitude was ≥ 30, then transect performance was deemed poor as it might limit usability significantly (Table 3). The expert-based choice of these values is discussed in section 5.5 below. Second, a test was performed to determine if increasing cross-sectional sampling by a factor of 10 yielded an increase in HG performance relative to HT baseline power function exponent values by a corresponding factor of 10 (i.e., a linear response). Third, the cross section whose power function exponents were closest to those of the corresponding HT functions was identified and the percent error in exponents was computed. Finally, the sum of the power function exponents and the geometric mean of the coefficients were computed and the deviation from unity assessed as a check on mass conservation. As explained in section 1.1, these derived metrics for some HG functions and all the HT functions are not required to equal one, but it was interesting to see which analyses yielded metrics closest to one.

4. Results

4.1. Segment results

Segment-scale log-linear plots revealed a wide variance between cross sections (Figs. 3A, D, G). Minimum and maximum cross-sectional values from the 100-m sampling spanned as much as 1.5 orders of magnitude at a given discharge, while the HT and HG segment-scale average hydraulics were within one order of magnitude over

UNCORRECTED FINAL MANUSCRIPT

the entire range of discharges. At the lowest flow of 8.5 m^3/s, the minimum and maximum values for width, depth, and velocity defined the ranges of 20–137 m, 0.16–3.82 m, and 0.04–1.40 m/s, respectively; whereas at bankfull discharge of 141.6 m^3/s the values ranged from 29 to 242 m, 0.64 to 4.29 m, and 0.47 to 2.53 m/s, respectively. Therefore, the corresponding relative change in range between the lowest and highest discharge was 96 m, -0.01 m, and 0.70 m/s, respectively. The spread of values in Figs. 3D and 3G can be visually misleading because of the logarithmic axes; only depth has a reduced range over the set of flows. Visually, the 100-m sampling performed better than the 1-km sampling for width, depth, and velocity; width near-census (i.e., 6-m) and 100-m results are indistinguishable. Interestingly, maximum segment depth drops slightly as discharge increases from 56.6 to 70.8 m^3/s, but stays relatively constant over the entire range of flows. Both 100-m and 1-km sampling methods overestimate velocity for nearly the entire range of flows.

The segment power regression exponents and coefficients for each sample method are presented in Table 3. The sum of width, depth, and velocity exponents is 0.99 for all three sampling approaches. The HT product of the coefficients is closest to 1 (1.06 vs 1.16 and 1.19 for HT, 100-m HG, and 1-km HG, respectively), which means that sampling creates a systematic shift upward in hydraulic values for the lowest flows. The 100-m sampling results for the segment outperformed the 1-km sampling as evidenced by the lower percent error magnitudes for all hydraulic regression parameters. All segment regression parameters derived from stations were below an absolute 50%error, with the exception of the 1-km sampling *k* value (92.64).

UNCORRECTED FINAL MANUSCRIPT

383 *4.2. Reach results*

384 Each reach has a dedicated column of log-linear plots in Fig. 4. The denser 100-
385 m sampling better approximated HT values than the 1-km sampling, except for
386 Timbuctoo Bend velocity (Fig. 4I) and at low flows for Marysville depth (Fig. 4D) and
387 velocity (Fig. 4G). The range of hydraulic values increased with discharge for most
388 combinations of river reach and hydraulic variable. The relative change in range
389 between the lowest and highest discharge for width, depth, and velocity, respectively,
390 was: 65 m, 0.20 m, and 0.42 m/s for Marysville; 90 m, 0.22 m, and -0.01 for DPD; and
391 24 m, -0.01 m, and 0.53 m/s for Timbuctoo Bend. A pattern consistent with all three
392 reaches was identified: if a HG sampling method overestimated depth for a majority of
393 flows relative to HT, then it also underestimated velocity, and vice versa. For instance,
394 Marysville 100-m and 1-km samplings of depth were low and high, respectively;
395 whereas those for velocity were high and low, respectively. In addition, cross-sectional
396 sampling along DPD and Timbuctoo Bend mostly underestimated depth and
397 overestimated velocity.

398 Reach-scale HT regression parameters with the exception of c were similar
399 between Marysville (e.g., b = 0.12) and Timbuctoo Bend (e.g., b = 0.14) (Table 3),
400 indicating that hydraulics responded similarly to increasing flow. Marysville and
401 Timbuctoo Bend had identical f values, therefore the rates at which depth increased as
402 a function of discharge was equal. While the sum of b, f, and m was always within 0.05
403 from unity for all reach scale sample methods, the product of a, c, and k ranges were
404 0.99–1.14, 1.10–1.23, and 1.20–1.44 for near-census, 100-m, and 1-km, respectively.
405 For Marysville and DPD, the product of regression coefficients and sum of regression

UNCORRECTED FINAL MANUSCRIPT

406 exponents strayed more from one as station sample density decreased.

407 The percent errors between HG and HT results revealed that cross-sectional
408 sampling consistently overestimated reach *f* and *k* values and underestimated *c* and *m*
409 values relative to the benchmark near-census results (Table 3). Otherwise, the percent
410 error appeared random and unpredictable, ranging from 0.71 to 158.7%.

411 Ternary plots showed how regression exponent combinations vary between
412 cross sections and longitudinally averaged river regions (Fig. 5). Points on the ternary
413 diagrams in Figs. 5A, B, and B represent individual cross sections located along that
414 reach. Reaches contained a minimum of 49 stations spaced every ~ 100 m (Table 2). In
415 general, few points fell below $m = 0.2$ or above $b = 0.5$, which connotes that as
416 discharge increases, slow velocity increases and fast width increases are uncommon.
417 There was considerable scatter between points of any given geomorphic reach, but
418 DPD was the most evenly dispersed. The DPD points were spread over the center of
419 the diagram where *b*, *f*, and *m* are roughly equal. Marysville and Timbuctoo Bend data
420 exhibited clustering at high *m* and low *b* regions, which indicate high rates of velocity
421 increase and low rates of width increase with discharge.

422 The *b-f-m* combinations for HG and HT vary for segment and reach scales (Fig.
423 5D). The HT results, indicated by squares, best represent hydraulics for that spatial
424 scale by definition. Segment scale results for all HG sampling techniques are situated
425 between the reach results as one would expect.

426

427 *4.3. Morphological units*

428 Riffle and pool hydraulics were plotted as a function of discharge for each

UNCORRECTED FINAL MANUSCRIPT

sampling method in Fig. 3. The minimum, maximum, and cross-sectional widths that appear in Figs. 3B and 3C represent individual cross sections that passed through the MU centroid. The abrupt reduction in minimum riffle width (Fig. 3B) and increase in maximum riffle velocity (Fig. 3H) that occurs at 19.82 m^3/s was because of the exclusion of Englebright dam reach hydraulics from the data set for flows less than that value (excluded because of a lack of a stage-discharge relation for low base flows influenced by a unique natural hydraulic structure at the end of that reach), as this reach is a narrow bedrock/boulder canyon, so its different character systematically influences the HG and HT results the same way. Cross-sectional sampling underrepresented the average LYR pool depth across all flows (Fig. 3F). This is explained by the fact that sampling of an MU by cross section includes the shallow near-bank pixels that by definition are not strictly part of pools and riffles (Wyrick and Pasternack, 2014). This is an important reason why laterally explicit MUs and HT analysis represents a refinement in understanding river morphometry over HG analyses that do not resolve the lateral limits of in-channel fluvial landforms.

The HT regression parameters for riffle and pool were very distinct (Table 3) and tended to represent the extreme parameters determined for the LYR. For instance, the lowest reported *c* value (0.07) and highest reported *f* value (0.64) characterized riffles as the overall shallowest landform having the most rapid rate of discharge-dependent depth increase. Additionally, riffles displayed the highest low-flow velocity (k = 0.35) and slowest velocity increase per unit discharge (m = 0.32) (Table 3). Pools were nearly opposite from riffles in that they exhibited a slow depth increase and rapid velocity increase with increasing discharge indicated by f = 0.19 and m = 0.74, respectively. By

UNCORRECTED FINAL MANUSCRIPT

452 comparison, the HG depth exponent, *f*, had a negative percent error for both MUs,
453 unlike any other spatial scale methodology comparison. As with previous spatial scales,
454 the MU percent error magnitude seemed random.
455 Two distinct HG data clusters represented pool and riffle cross sections (Fig. 6).
456 Pool points were tightly packed compared to riffle points. The difference in point density
457 likely results from the tendency for pools to more fully span the channel. In essence,
458 pool cross sections tended to be more representative than those situated across riffles.
459 The HT result in each case plotted outside of the main cluster owing to higher *f* and *m*
460 values, indicating that depth and velocity increased at a greater rate with flow than
461 shown by HG sampling.
462
463 *4.4. Sampling resolution test result*
464 The HG results for the segment and one reach (DPD) moved toward the near-
465 census mark as sample density increased from 1 km to 100 m, whereas those for
466 Timbuctoo Bend and Marysville reaches shifted but did not appear any closer to the
467 near-census benchmark (Fig. 5D). The degree of exponent values shifting toward the
468 HT benchmark relative to a tenfold increase in sampling was nonlinear 11 times and
469 linear once. Only the segment scale *b* exponent exhibited a linear trend because the
470 absolute difference between the HT and 1-km marks was 0.021 and the difference
471 between the HT and 100-m marks was 0.0021. Of the nonlinear shifts, *m* and *f* were
472 consistently slower than linear, and *b* was faster than linear for each reach. That is, 100-
473 m sampling *b* values yielded less than one-tenth of the error than those from 1-km
474 sampling. Also, the transitions from 1-km HG to 100-m HG to HT for Timbuctoo Bend

UNCORRECTED FINAL MANUSCRIPT

and Marysville reaches had a similar pattern to each other (Fig. 5D).

4.5. Representative station test result

No cross section's HG exponents exactly matched those from its HT benchmark, but each case yielded a cross section reasonably close (Table 5). Of 16 exponent values computed, only one exceeded 10% absolute error and three were between 5-10% absolute error, with the rest within 5%. Timbuctoo Bend and pool yielded the closest representation, with a *b-f-m* distance of 3.28 and 3.35%, respectively. As illustrated in Fig. 5, few cross sections are close to the HT benchmark. How one would ever find the very small number of representative cross sections in practice among a set with so much variance is unknown.

4.6. Continuity results

The sum of power function exponents and the geometric mean of the coefficients are normally used in HG studies to verify continuity at a cross section. However, in this HT study, neither the sums of exponents or products of coefficients were derived from a single station, yet they still come close to unity. Across every spatial scale and sample scheme, *b+f+m* values were no more than 0.05 off of the ideal mark. As for *a*c*k* values, the HT values were closer to one than any form of cross section sampling scheme for HG. This bodes well for the HT method.

UNCORRECTED FINAL MANUSCRIPT

5. Discussion

5.1. Hydraulic variability

Gravel-cobble river hydraulics in the LYR, as revealed through near-census mapping and 2D modeling, exhibited a high degree of lateral and longitudinal variability such that few cross section samples were alike, as was evident by the significant spread of cross-sectional HG exponents for each reach (Figs. 5A, B, C). Cross sections sampled a variety of diverse landforms along the LYR, including meanders, training levee-confined areas, bedrock constrictions, riffle–pool sequences, relatively steep and narrow bedrock-confined areas, and subwidth-scale MUs of diverse shapes and sizes. On average there were eight MUs across the bankfull channel (Wyrick and Pasternack, 2014).

At base flow, regions of slow moving water such as pools, backwaters, and slackwaters contrasted with swift, turbulent water such as riffles and chutes, representing velocity extremes. Looking at the slopes of the HG functions for the 18 pairs of minimum and maximum cross sections (Figs. 3–4), 10 show a convergence from base to bankfull flow, indicating a smoothing of hydraulics. However, the fact that almost as many show no change or a divergence in slopes indicates that as flow increases, new landform features are added to the wetted area maintaining hydraulic heterogeneity. This is counter to the conventional wisdom that relative roughness (depth:grain size) and thus hydraulic heterogeneity decreases with increasing discharge. Abu-Aly et al. (2013) reported a continuing maintenance of hydraulic heterogeneity for a wide range of LYR floods.

One could argue that each cross section in a river would produce a unique

UNCORRECTED FINAL MANUSCRIPT

519 combination of discharge-dependent hydraulics. Two cross sections could have the
520 same wetted width, average depth, or average velocity for a given flow, but given
521 multiple scales of landform heterogeneity in a natural river segment transitioning from a
522 mountain to a lowland, how likely is it that both stations would exhibit the same values
523 for all three variables for the range of flows up to bankfull? This is not likely, as a
524 plethora of interdependent factors influencing the channel dimensions (e.g., underlying
525 and exposed lithology, bed/bank material size, vegetation, flow regime, fluvial
526 landforms, and topographic change processes), which in turn alter flow hydraulics (Abu-
527 Aly et al., 2013). The point is that at-a-station HG relationships on a diverse river like the
528 LYR vary wildly across different transects — perhaps far more than geomorphologists
529 have wanted to admit in light of practical constraints on how much sampling can be
530 done.
531
532 *5.2. HG sampling versus HT near-census*
533 This study used a maximum of 354 cross sections at the segment scale and
534 relatively high numbers (49–58 cross sections) at the reach scale for reaches of 5–6 km
535 length. Few, if any, geomorphologists measure 50–60 cross sections for at-a-station HG
536 relation development in a 5–6 km reach, let alone make observations at 20 different
537 discharges spanning an order of magnitude. To put the sampling density used in this
538 study into perspective, examples of at-a-station HG sampling were gleaned from the
539 professional literature in which at-a-station HG relations were used for river
540 management. As an example to highlight the typical amount of discharge sampling, the
541 use of at-a-station HG relations for 1D physical habitat simulation are likely the most

UNCORRECTED FINAL MANUSCRIPT

widespread practical application of this method. The protocols for these professional studies call for making observations at 1–3 discharges — ideally one for low, mid, and high flows (Payne and Bremm, 2003; Moir et al., 2005), compared to the 20 done herein. Also for habitat assessment studies, Payne et al. (2004) reported that 18–20 transects are suitable to characterize hydraulics well enough to define weighted usable area relationships that statistically sample how much physical habitat is present over a range of flows. After thorough evaluation of the 37.42-km lower Feather River segment, the phase two PHABSIM instream flow study used 53 transects (i.e., 8 per 6 km) (Payne, 2004). For the PHABSIM joint instream flow relicensing study for the Yuba, Bear, and Drum-Spaulding projects (http://www.eurekasw.com/DS/default.aspx; see study 2.3.2), hydraulic measurements and estimations were made for 81 transects along ~ 66 km (i.e., 7 per 6 km) of the South Yuba River.

Considering beyond HG applications, a more basic use of cross sections involves simply mapping them for use in 1D model studies, and even for that basis in which no flow-specific data is required, far fewer cross sections are commonly measured than were used in this study. That can be dictated by the interpreted locations of unevenly spaced hydraulic controls. For example, Gibson et al. (2010) performed a 1D numerical model for 32.2 km of the gravel and sand bedded Cowlitz River as part of an evaluation of sedimentation of material derived from the Mount St. Helens eruption of 1980. Sediment transport prediction is a highly nonlinear function of depth and velocity, so the need for accurate hydraulics is crucial. In that study, 95 unevenly spaced cross sections were used, which is equivalent to 18 per 6 km. Partridge and Baker (1987) used a 1D numerical model with 23 unevenly spaced cross

UNCORRECTED FINAL MANUSCRIPT

565 sections to study flood hydraulics in a 4.4-km, bedrock-confined segment of the Salt
566 River in Arizona (equivalent to 31 per 6 km). These high numbers are still substantially
567 lower than the numbers used in this study and do not involve hydraulic observations at
568 all the transects as would be necessary for HG relation development, so they represent
569 the typical upper limit done in the field in practice by geomorphologists and river
570 engineers.

571 Based on the results of this study, in several instances normal density and
572 extremely high density station-based sampling approaches performed poorly relative to
573 the near-census baseline, which is remarkable. Cases where both sampling schemes
574 produced percent error magnitudes relative to the HT reference over the poor
575 performance threshold of 30 included segments *f* and *k*, Marysville *f*, and Timbuctoo
576 Bend *f*. Segment scale *k* percent errors were especially high at 48.59 and 92.64 for 100-
577 m and 1-km, respectively. The significance of these findings for a high density of cross
578 sections is that cross section sampling at any spacing is unlikely to yield accurate
579 results to characterize river hydraulics.

580

581 *5.3. 100-m versus 1-km sampling*

582 The chances of cross-sectional HG results approximating HT results is expected
583 to increase with increased sample density. The LYR segment and three geomorphic
584 reaches were sampled using transects spaced every 100 m and 1 km to test whether
585 increasing sample density by a factor of 10 improved results. All segment scale
586 regression constants estimated from the 100-m sampling had a lower percent error
587 magnitude than those estimated with the 1-km sampling, which indicated that a

UNCORRECTED FINAL MANUSCRIPT

588 sampling with 36 cross sections was not sufficient to characterize segment scale
589 hydraulics compared to HT results that were defined as the benchmark best results.
590 Whether some number between 36 and 354 would be adequate was not systematically
591 evaluated, but a tenfold increase in samples yielded a 10-, 1.4-, and 1.8-fold decrease
592 in the deviation for segment-scale *b*, *f*, and *m*, respectively. Meanwhile, in most cases
593 HG reach-scale results from 100-m sampling better matched HT results compared to
594 the 1-km sampling, as indicated by the lower percent error magnitudes; the exceptions
595 included *c*, *m* and *k* values for Marysville reach, *m* and *k* values for Timbuctoo Bend
596 reach, and the *f* value for DPD reach (Table 3). Thus, improvement was not universal
597 despite a tenfold increase in sampling, which is quite remarkable. Based on these
598 findings, the traditional expectation that more sampling better approximates the
599 population does hold up for HG relations, but it is not universally true and does not scale
600 linearly to the extent that our data allowed for that to be evaluated.
601
602 *5.4. Nonrepresentative samples*
603 Typically, the purpose of sampling is to get at the central tendency of the
604 population. Fluvial geomorphologists may theorize about and search for a station that is
605 representative of some reach. But, does reach representativeness refer to the mean
606 state and/or to the full range of reach hydraulic variability? It seems that a single cross
607 section could only represent the mean condition of the sample population and would not
608 be able to characterize the complete hydraulic variability.
609 Near-census sampling and HT analysis provides closer to true average than any
610 cross section based sampling method and HG analysis. An individual station might

UNCORRECTED FINAL MANUSCRIPT

611 come close to the average, but if the average is not known in the first place, how does
612 one select or verify that station? Fluvial scientists rely on their expertise, but some luck
613 and risk are still involved in selecting the average site. Very few cross sections came
614 close to representing some greater spatial scale in this study. Unless by sheer luck, no
615 single cross section could ever represent the hydraulics of multiple scales (both
616 segment and reach) on the LYR, as the near-census *b-f-m* results for each sample were
617 all distinct (Fig. 5). There is value in averaging across stations as it produces results
618 that are closer to the target near-census HT *b-f-m* points (Fig. 5D). Similarly, with
619 respect to MUs, averaging multiple cross-sectional values got closer to the near-census
620 results than most individual stations.
621
622 *5.5. How much HG error is okay?*
623 The assessment as to how much at-a-station HG error is okay is largely
624 unexplored in science and engineering. Because it depends on what purpose the HG
625 relations will be used for, there is unlikely to be a single universal benchmark for all
626 coefficients and exponents in all applications. Anecdotally, academic sediment and river
627 scientists are often satisfied with answers to within a factor of two, but now that bankfull
628 HG relations are widely used to specific design channel dimensions, such as in the
629 'natural channel design' methodology (Rosgen and Silvey, 1996; Rosgen, 1998, 2001)
630 and the new synthetic river valley methodology (Brown et al., 2014), it is not an
631 academic question, but an essential challenge determining whether restoration
632 investments are meaningful or wasted.
633 Although benchmarks for the required accuracy of at-a-station HG relations in

UNCORRECTED FINAL MANUSCRIPT

634 professional practice do not exist, some studies suggest some levels of specificity
635 required for bankfull channel dimensions. For example, Jackson et al. (2015) evaluated
636 how much wider the channel would have to be to eliminate the hydraulic velocity
637 reversal at Keller's (1971) classic Dry Creek site. They found that given the weak state
638 of that velocity reversal, widening the pool by just 10% eliminated the occurrence of a
639 mean velocity reversal. However, when the strong differentiation between grain sizes
640 was accounted for by using the observational substrate data for that site (i.e., coarse
641 sediment on riffle sand fine sediment in pools) and switching from mean velocity to
642 mean Shields stress, then even with a widening of 30% the strong Shields stress
643 reversal could not be eliminated.

644 Another example comes from the design of the restructured and rescaled
645 channel in the Robinson Reach of the lower Merced River, CA. In this project,
646 geomorphic methods were used to obtain the reach-scale channel width but then to
647 increase the velocity over riffles to provide suitable hydraulics for salmonid spawning,
648 hydraulic engineers specified that riffle width be reduced relative to pool width, and that
649 was done. This is the exact opposite of what is advised geomorphically in order to have
650 self-sustaining riffles and pools composed of roughly the same substrate size, in light of
651 the flow convergence routing mechanism proposed by MacWilliams et al. (2006) and
652 supported subsequently by Caamaño et al. (2009) and Sawyer et al. (2010).
653 Conceptually, unforced pools need to be width constricted relative to riffles (which in
654 turn are vertically constricted at low flow) in order for there to be a stage-dependent shift
655 in the position of peak Shields stress from base flows to floods. Harrison et al. (2011)
656 reported that mean bankfull pool width in the reach was only ~ 7–8% greater than mean

UNCORRECTED FINAL MANUSCRIPT

riffle width, but more relevant to this study is the fact that for the base-flow condition aerial imagery of the as-built condition shows that the typical difference between riffle and pool width was ~ 30%. Thus, there is an at-a-station hydraulic geometry effect present in the designed channel. The consequence has been that sufficient quantities of spawning substrate have eroded off the riffles and deposited in the pools to fundamentally restructure channel geometry different from the design (Harrison et al., 2011). Besides this being present in the DEM difference results of Harrison et al. (2011), readers can see it for themselves by using Google Earth to view the reach in aerial imagery from 2004 to 2011; it is evident that the base-flow wetted area of the pools decreased substantially for many of them, reversing the width difference to make the riffles wider than the pools (see for example the change in pool width at latitude 37.4804°, longitude -120.4828°). These examples suggest that even a difference of ~ 10% in mean bankfull width can have dramatic negative effects relative to design expectations. Hopefully over time more research will emerge from river restoration studies to help constrain how resilient channel designs are in the face of error in HG relations.

In this study, percent errors found for transect-derived regression exponents and coefficients relative to the near-census benchmark were highly differentiated (Table 3). Negative/positive percent errors correspond to underestimation/overestimation of regression constants by transect-based sampling. The thresholds of 10% and 30% error magnitude represent the estimated thresholds for poor and good sampling performance with the acknowledgment that acceptable error is project-specific: ≤ 10% is considered good, and ≥ 30% is considered poor. All width (*b* and *a*) parameters from 100-m

UNCORRECTED FINAL MANUSCRIPT

680 regression constants were ≤ 10% error of HT (Figs. 3A, B, C; 4A, B, C), which indicated
681 that 100-m spaced transect sampling was well suited for determining width-discharge
682 relations, yet that density of sampling is not used in practice. In any case, percent errors
683 associated with depth and velocity parameters suggest otherwise. Station-derived depth
684 exponents, *f*, performed poorly for all reach and segment scales except DPD, as
685 indicated by corresponding percent error magnitudes ≥ 30 (Table 3). Depth coefficients,
686 *c*, were below the 30% error magnitude threshold for all scales except for riffle MU and
687 1-km segment and Timbuctoo Bend reach. Velocity exponents, *m*, performed well
688 overall as only one case was above the poor performance threshold (1-km DPD), four
689 cases were classified as good performance, and the five remaining unclassified cases
690 tended toward the good performance threshold (i.e., values were between -14 and 14)
691 (Table 3). Lastly, with respect to the velocity coefficients, *k*, three-quarters of the 100-m
692 samples, one-half of the 1-km samples, and none of the MU samples surpassed the
693 percent difference magnitude of 30. Overall, by these standards many sampling
694 schemes poorly represented the power parameters produced by near-census HT, but
695 this was especially the case for *f* and *k*. Table 4a confirms that *f* and *k* have the greatest
696 average absolute percent error relative to the HT benchmark.

697 The modal class as reported by Park (1977) for at-a-station HG exponents *b*, *f*,
698 and *m* was 0.0–0.1, 0.3–0.4, and 0.4–0.5, respectively. Assume the true HT exponents
699 of some river reach were exactly the upper bound of these modal classes, such that *b* =
700 0.1, *f* = 0.4, and *m* = 0.5. Suppose a researcher went to sample that same reach to
701 determine those constants. If the average reach-scale regression exponent absolute
702 percent errors with respect to the near-census HT values in Table 4b were applied to

UNCORRECTED FINAL MANUSCRIPT

703 the data, one would expect there to be roughly 20, 30, and 15% error for *b*, *f*, and *m*,
704 respectively. Based on the signs of error in Table 3, *b* error could be positive or
705 negative, *f* error positive, and *m* error negative. Based on these assumptions, the
706 sample error would be 0.02, 0.12, and 0.08 for *b*, *f*, and *m*, respectively. Consequently,
707 the researcher would produce *b*, *f*, and *m* values of $b = 0.8$ or 1.2, $f = 0.52$, and $m =$
708 0.42. These regression results misrepresent the discharge-dependent reach-scale
709 hydraulics, which could have varying negative effects depending on the application.
710
711 *5.6. Comparing among literature*
712 Several issues when comparing HG results across studies, most of which stem
713 from different forms of sampling bias. In general, it is not advisable to compare HG
714 exponents across studies unless there is sufficient detail on how the data were obtained
715 and processed, and that those details satisfy the researcher's standards for
716 comparison. It may prove helpful if researchers publish the decisions used to produce
717 HG relationships for a specific study as supplemental materials, perhaps using a
718 transparent decision tree (e.g., Fig. 1). Spatially explicit HT alleviates many of the
719 decision-making pressures associated with fieldwork and shifts decisions to the end as
720 part of an analysis workflow open to scrutiny by stakeholders and peer reviewers. It
721 requires some explanation of hydrodynamic modeling techniques, which traditional HG
722 does not; but such models are rapidly becoming standard tools for geomorphology.
723 Variation in HG or HT values could arise from model choice and variable roughness
724 settings (Stewardson, 2005). Hydraulic topography would allow for more types of
725 hydraulics comparisons if it were widely adopted.

UNCORRECTED FINAL MANUSCRIPT

726

727 *5.7. Simulated sampling choices*

728 Given the comparison goals of this study, the cross section sampling process
729 from a near-census data set posed some issues. First is that there were no physical
730 limitations to where samples could be placed along a river, nor were there serious time
731 constraints now that the data had been collected and models run. The near-census
732 model data sets simply provided so much information about the LYR that any sort of
733 attempt to sample the river as a field person would be unfair. To avoid simulating
734 surveyor bias and expert judgment inherent in making field decisions, the cross-
735 sectional sampling for this study was based on uniform spacing. The uniform
736 longitudinal sampling carried out did not align with a periodic river characteristic such as
737 riffle–pool sequences or meanders, and thus the aggregated larger scale results should
738 not be skewed toward the condition of that feature.

739

740 *5.8. Flow direction considerations*

741 Many rivers are nonprismatic and have highly variable hydraulics with lateral
742 shear zones, eddies, backwaters, and slack waters. These deviations from steady and
743 uniform flow limit the ability of cross sections and traditional HG analysis to represent
744 hydraulics and fluvial geomorphology. Some of the nonuniformity issues include
745 averaging of flow velocities that are not pointed in one direction, which can misrepresent
746 the velocity data and thereby conveyance. As flows change, so does the wetted
747 perimeter of the channel. In general, river widths are an approximation because they
748 are based on field-based visual determination of the orthogonal direction (usually for the

UNCORRECTED FINAL MANUSCRIPT

top wetted width or guesstimated bankfull position) on the day of measurement, even when banks are not parallel or easily visualized from the ground. In this study station lines were selected to be orthogonal to the valley centerline given high thalweg tortuosity, which could potentially overestimate bankfull width, as transect misdirection can only result in widths greater than what is actually true. However, the fact that the HT relations yielded exponents summing nearly to one suggests that this uncertainty is not a significant constraint despite its conceptual potential to be a problem.

6. Conclusions

Near-census river science and the HT analysis proposed herein eliminate several sample- and assumption-based inconsistencies for traditional HG analysis. Moving beyond transect-based HG field methods is inevitable given the rate of technological development — the argument that near-census topographic mapping and spatially explicit hydrodynamic modeling is infeasible or excessively costly is rapidly breaking down, while the cost of field campaigns for selecting and measuring individual cross sections (including hydraulics at numerous discharges) remains high to infeasible. The analyses possible with near-census spatially explicit data sets are vast and not limited to HG type. A near-census approach would allow HT researchers to pinpoint river regions like spawning/rearing fish habitat, steep banks vulnerable to collapse, or buffered zones around vegetation species of interest. The data could be queried and divided in any fashion.

Overall, HG analyses performed poorly with respect to the HT benchmark. Percent error magnitudes for power regression parameters derived from cross sections were often above 30% compared to HT baseline results, which could be acceptable

UNCORRECTED FINAL MANUSCRIPT

depending on the application. When undertaking complex environmental studies, understanding hydraulic parameters is essential, especially as researchers and practitioners strive to recreate river ecosystems. All sampling schemes provide an incomplete picture of reality, so it is important to base environmental sampling design on the questions to be answered, which could require differing temporal and spatial resolution, which near-census HT can provide.

Acknowledgements

Primary funding for this study was provided by the Yuba County Water Agency and the Yuba Accord River Management Team (Award #201016094). This project was also supported by the USDA National Institute of Food and Agriculture, Hatch project number #CA-D-LAW-7034-H. We appreciate Anne Senter, Carlos Puente, Michael Strom, Matthew Vaughan, and Betsy Bamberger for providing valuable feedback during the early stages of this project. We also thank Professor Paul Bates (University of Bristol) for a helpful manuscript review prior to submission as well as an anonymous peer review and Geomorphology editor Richard Marston for further revisions.

References

Abu-Aly, T.R., Pasternack, G.B., Wyrick, J.R., Barker, R., Massa, D., Johnson, T., 2013. Effects of LiDAR-derived, spatially distributed vegetation roughness on two-dimensional hydraulics in a gravel-cobble river at flows of 0.2 to 20 times bankfull. Geomorphology, 206, 468-482.

Andrews, E.D., 1984. Bed-material entrainment and hydraulic geometry of gravel-bed rivers in Colorado. Geological Society of America Bulletin, 95(3), 371-378.

Barker, J.R., 2011. Rapid, abundant velocity observation to validate million-element 2D hydrodynamic models. M.S. Thesis, University of California, Davis, CA.

UNCORRECTED FINAL MANUSCRIPT

799 Brasington, J., Rumsby, B.T., McVey, R.A., 2000. Monitoring and modeling
800 morphological change in a braided gravel-bed river using high-resolution GPS-
801 based survey. Earth Surface Processes and Landforms 25(9), 973-990.

802 Brown, R.A., Pasternack, G.B., 2008. Engineered channel controls limiting spawning
803 habitat rehabilitation success on regulated gravel-bed rivers. Geomorphology,
804 97(3-4), 631-654.

805 Brown, R.A., Pasternack, G.B., 2009. Comparison of methods for analysing salmon
806 habitat rehabilitation designs for regulated rivers. River Research and
807 Applications, 25(6), 745-772.

808 Brown, R. A., Pasternack, G. B., Wallendar, W. W. 2014. Synthetic river valleys:
809 creating prescribed topography for form-process inquiry and river rehabilitation
810 design. Geomorphology 214: 40-55.

811 Caamaño, D., Goodwin, P., Buffington, J.M., Liou, J.C., Daley-Laursen, S., 2009.
812 Unifying criterion for the velocity reversal hypothesis in gravel-bed rivers. Journal
813 of Hydraulic Engineering, 135(1), 66-70.

814 Carley, J.K., Pasternack, G.B., Wyrick, J.R., Barker, J.R., Bratovich, P.M., Massa, D.A.,
815 Reedy, G.D., Johnson, T.R., 2012. Significant decadal channel change 58–
816 67years post-dam accounting for uncertainty in topographic change detection
817 between contour maps and point cloud models. Geomorphology, 179, 71-88.

818 Copeland, R.R., McComas, D.N., Thorne, C.R., Soar, P.J., Jonas, M.M., 2001.
819 Hydraulic design of stream restoration projects, U.S. Army Corps of Engineers,
820 Baltimore, MD.

821 Gibson, S., Nygaard, C., Sclafani, P., 2010. Mobile Bed Modeling of the Cowlitz River
822 Using HEC-RAS: Assessing Flood Risk and Impact due to System Sediment,
823 2nd Joint Interagency Sediment and Hydrology Conference, Las Vegas, Nevada,
824 USA.

825 Gleason, C.J., Smith, L.C., 2014. Towards global mapping of river discharge using
826 satellite images and at-many-stations hydraulic geometry. Proceedings of the
827 National Academies of Sciences, 111(13), 4788-4791.

828 Harrison, L., Legleiter, C., Wydzga, M., Dunne, T., 2011. Channel dynamics and habitat
829 development in a meandering, gravel bed river. Water Resources Research,
830 47(4).

831 Hilldale, R.C., Raff, D., 2007. Assessing the ability of airborne LiDAR to map river
832 bathymetry. Earth Surface Processes and Landforms 33(5), 773-783.

UNCORRECTED FINAL MANUSCRIPT

833 Hogan, D.L., Church, M., 1989. Hydraulic geometry in small, cosatal streams —
834 progress toward quantification of salmonid habitat. Canadian Journal of Fisheries
835 and Aquatic Sciences, 46(5), 844-852.

836 Horritt, M.S., Bates, P.D., 2002. Evaluation of 1D and 2D numerical models for
837 predicting river flood inundation. Journal of Hydrology, 268(1), 87-99.

838 Jackson, J.R., Pasternack, G.B., Wheaton, J.M., 2015 . Virtual manipulation of
839 topography to test potential pool-riffle maintenance mechanisms.
840 Geomorphology 228, 617-627

841 Jowett, I.G., 1998. Hydraulic geometry of New Zealand rivers and its use as a
842 preliminary method of habitat assessment. Regulated Rivers: Research and
843 Management, 14(5), 451-466.

844 Keller, E.A., 1971. Areal sorting of bed-load material: the hypothesis of velocity reversal.
845 Geological Society of America Bulletin, 82(3), 753-756.

846 Knighton, A.D., 1974. Variation in width-discharge relation and some implications for
847 hydraulic geometry. Geological Society of America Bulletin, 85(7), 1069-1076.

848 Knighton, A.D., 1975. Variation in at-a-station hydraulic geometry. Journal of Science,
849 275, 186-218.

850 Knighton, A.D., 1998. Fluvial Forms and Processes: A New Perspective. Arnold, Hodder
851 Headline, PLC.

852 Langbein, W.B., 1964. Geometry of river channels. Journal of the Hydraulics Division
853 Proceedings of the American Society of Civil Engineers, 90, 301-312.

854 Leopold, L.B., Maddock, T., 1953. The hydraulic geometry of stream channels and
855 some physiographic implications, United States Geological Survey, Washington,
856 D.C., USA.

857 Leopold, L.B., Wolman, M.G., 1957. River channel patterns: braided, meandering, and
858 straight, US Government Printing Office Washington, DC.

859 MacWilliams, M.L., Wheaton, J.M., Pasternack, G.B., Kitinidis, P.K., Street, R.L., 2006.
860 The Flow Convergence-Routing Hypothesis for Pool-Riffle Maintenance in
861 Alluvial Rivers. Water Resources Research, 42(W10427),
862 doi:10.1029/2005WR004391.

863 Merigliano, M.F., 1997. Hydraulic geometry and stream channel behavior: a uncertain
864 link. Journal of the American Water Resources Association, 33(6), 1327-1336.

UNCORRECTED FINAL MANUSCRIPT

865 Moir, H., Gibbins, C., Soulsby, C., Youngson, A., 2005. PHABSIM modelling of Atlantic
866 salmon spawning habitat in an upland stream: testing the influence of habitat
867 suitability indices on model output. River Research and Applications, 21(9),
868 1021-1034.

869 Navratil, O., Albert, M.B., 2010. Non-linearity of reach hydraulic geometry relations.
870 Journal of Hydrology, 388(3-4), 280-290.

871 Ozdemir, H., Sampson, C.C., de Almeida, G.A.M., Bates, P.D., 2013. Evaluating scale
872 and roughness effects in urban flood modelling using terrestrial LIDAR data.
873 Hydrology and Earth System Sciences, 17(10), 4015-4030.

874 Park, C.C., 1977. World-wide variations in hydraulic geometry exponents of stream
875 channels — analysis and some observations. Journal of Hydrology, 33(1-2), 133-
876 146.

877 Partridge, J., Baker, V.R., 1987. Palaeoflood hydrology of the Salt river, Arizona. Earth
878 Surface Processes and Landforms, 12(2), 109-125.

879 Pasternack, G.B., 2009. Appendix X: Specific Sampling Protocols and Procedures for
880 Topographic Mapping, The Lower Yuba River Accord Planning Team, Marysville,
881 CA.

882 Pasternack, G.B. 2010. Existing information attachment: fluvial geomorphology
883 downstream of USACE's Englebright Dam. Prepared for Yuba County Water
884 Agency, Yuba River Development Project, FERC Project No. 2246.

885 Pasternack, G.B., 2011. 2D Modeling and Ecohydraulic Analysis. Createspace, Seatle,
886 WA.

887 Pasternack, G.B., Tu, D., Wyrick, J.R., 2014. Chinook adult spawning physical habitat of
888 the lower Yuba River, Prepared for the Yuba Accord River Management Team.
889 University of California, Davis, CA.

890 Payne, T.R., 2004. Evaluation of project effects on instream flows and fish habitat,
891 Prepared for the California Department of Water Resources, Oroville Facilities.

892 Payne, T.R., Bremm, D.J., 2003. The influence of multiple velocity calibration sets on
893 the PHABSIM habitat index, Proceedings of International IFIM users workshop
894 (CD), pp. 1-5.

895 Payne, T.R., Eggers, S.D., Parkinson, D.B., 2004. The number of transects required to
896 compute a robust PHABSIM habitat index. Hydroécologie Appliquée, 14, 27-53.

UNCORRECTED FINAL MANUSCRIPT

Pitlick, J., Cress, R., 2002. Downstream changes in the channel geometry of a large gravel bed river. Water Resources Research, 38(10), 1216.

Rhodes, D.D., 1977. The b-f-m diagram: graphical representation and interpretation of at-a-station hydraulic geometry. American Journal of Science, 277, 73-96.

Richards, K.S., 1976a. Channel width and riffle–pool sequence. Geological Society of America Bulletin, 87(6), 883-890.

Richards, K.S., 1976b. Morphology of riffle–pool sequences. Earth Surface Processes and Landforms, 1(1), 71-88.

Rosgen, D.L., 1994. A classification of natural rivers. Catena, 22(3), 169-199.

Rosgen, D.L., 1998. The reference reach: a blueprint for natural channel design, Engineering Approaches to Ecosystem Restoration. ASCE, pp. 1009-1016.

Rosgen, D.L., 2001. A Stream Channel Stability Methodology, Proceedings of the Seventh Federal Interagency Sedimentation Conference, Reno, Nevada, pp. 18-26.

Rosgen, D.L., Silvey, H.L., 1996. Applied river morphology, 1481. Wildland Hydrology Pagosa Springs, CO.

Sampson, C.C., Fewtrell, T.J., Duncan, A., Shaad, K., Horritt, M.S., Bates, P.D., 2012. Use of terrestrial laser scanning data to drive decimetric resolution urban inundation models. Advances in Water Resources, 41(0), 1-17.

Sawyer, A.M., Pasternack, G.B., Moir, H.J., Fulton, A.A., 2010. Riffle–pool maintenance and flow convergence routing observed on a large gravel-bed river. Geomorphology, 114(3), 143-160.

Shields, F., Copeland, R., Klingeman, P., Doyle, M., Simon, A., 2003. Design for stream restoration. Journal of Hydraulic Engineering, 129(8), 575-584.

Singh, V.P., 2003. On the theories of hydraulic geometry. International Journal of Sediment Research, 18(3), 196-218.

Stewardson, M.J., 2005. Hydraulic geometry of stream reaches. Journal of Hydrology, 306(1-4), 97-111.

Turnipseed, P.D., Sauer, V.B., 2010. Discharge Measurements and Gaging Stations: U.S. Geological Survey Techniques and Methods book 3. Reston, VA.

UNCORRECTED FINAL MANUSCRIPT

927 Wadeson, R., 1994. A geomorphological approach to the identification and classification
928 of instream flow environments. Southern African Journal of Aquatic Science,
929 20(1-2), 38-61.

930 White, J.Q., Pasternack, G.B., Moir, H.J., 2010. Valley width variation influences riffle–
931 pool location and persistence on a rapidly incising gravel-bed river.
932 Geomorphology, 121(3), 206-221.

933 Williams, G.P., 1978. The hydraulic geometry of river cross sections — theory of
934 minimum variance. United States Department of the Interior; Geological Survey,
935 Washington D.C., USA.

936 Williams, R.D., Brasington, J., Vericat, D., Hicks, D.M., 2014. Hyperscale terrain
937 modelling of braided rivers: fusing mobile terrestrial laser scanning and optical
938 bathymetric mapping. Earth Surface Processes and Landforms, 39(2), 167-183.

939 Wolman, M.G., Brush, L.M., 1961. Factors controlling the size and shape of stream
940 channels in coarse noncohesive sands. U.S. Government Printing Office.

941 Wyrick, J.R., Pasternack, G.B., 2008. Modeling energy dissipation and hydraulic jump
942 regime responses to channel nonuniformity at river steps. Journal of Geophysical
943 Research: Earth Surface, 113(F3), F03003.

944 Wyrick, J.R., Pasternack, G.B., 2012. Landforms of the Lower Yuba River, Prepared for
945 the Lower Yuba River Accord Planning Team. University of California, Davis, CA.

946 Wyrick, J.R., Pasternack, G.B., 2014. Geospatial organization of fluvial landforms in a
947 gravel–cobble river: beyond the riffle–pool couplet. Geomorphology, 213, 48-65.

948 Xu, J.X., 2004. Comparison of hydraulic geometry between sand- and gravel-bed rivers
949 in relation to channel pattern discrimination. Earth Surface Processes and
950 Landforms, 29(5), 645-657.

951 Yuba Accord River Management Team (YARMT), 2010. Lower Yuba River Accord
952 Monitoring and Evaluation Program. Draft. June 28, 2010.

953 Zhang, M., Shen, Y., 2008. Three-dimensional simulation of meandering river based on
954 3-D RNG κ-ε turbulence model. Journal of Hydrodynamics, Ser. B, 20(4), 448-
955 455.

956

957

UNCORRECTED FINAL MANUSCRIPT

Table 1
Geomorphic reach data[a]

Geomorphic reach	Baseflow width (m)	Bankfull width (m)	Valley width[b] (m)	Bed slope[b] (%)	Substrate size[b] (mm)	Entrenchment ratio[b]	Width/ Depth[b]
Timbuctoo Bend	61	81	162	0.20	164	2.1	82
DPD	61	115	438	0.18	87	3.5	85
Marysville	52	67	148	0.05	40	2.6	23

[a] Mean widths were calculated for this study using the geometric mean of cross sections spaced 6.1 m along the valley centerline. The modeled discharge regimes were baseflow (24.9 m^3/s above Daguerre Point Dam (DPD) and 15.0 m^3/s below), and bankfull (141.6 m^3/s). Substrate size is the weighted mean grain size.

[b] From Wyrick and Pasternack (2012).

Table 2
Cross section data for the river segment and each geomorphic reach

Domain	Thalweg length (km)	Valley centerline (km)	6.1-m cross sections (#)	100-m cross sections (#)	1-km cross sections (#)
Segment	37.4	35.2	5735	354	36
Timbuctoo Bend	6.34	5.78	947	58	6
DPD	5.64	5.00	816	51	6
Marysville	5.33	4.97	790	49	5

Table 3
Summary table of coefficients and exponents for all combinations of hydraulic type, spatial scale, and methodology; the percent error quantifies how station-determined hydraulic geometry (HG) values deviate from the near-census hydraulic topography (HT) values

	Width		Depth		Velocity			
HT results	b	a	f	c	m	k	b+f+m	a*c*k
Segment	0.20	31.33	0.24	0.44	0.55	0.08	0.99	1.06
Marysville	0.12	35.25	0.18	0.96	0.70	0.03	1.01	0.99
DPD	0.28	25.62	0.29	0.29	0.42	0.15	0.99	1.08
Timbuctoo	0.14	38.88	0.18	0.54	0.66	0.05	0.98	1.14
Riffle	-	-	0.64	0.07	0.32	0.35	-	-
Pool	-	-	0.19	1.30	0.74	0.03	-	-
100-m cross-sectional HG results								
Segment	0.20	31.65	0.32	0.32	0.48	0.12	0.99	1.16
Marysville	0.13	34.21	0.25	0.72	0.62	0.04	0.99	1.10
DPD	0.28	26.19	0.33	0.25	0.38	0.18	0.99	1.18
Timbuctoo	0.14	39.62	0.26	0.38	0.58	0.08	0.98	1.23
1-km cross-sectional HG results								
Segment	0.22	30.65	0.35	0.26	0.42	0.15	0.99	1.19
Marysville	0.07	52.23	0.26	0.77	0.65	0.03	0.98	1.26
DPD	0.39	17.22	0.32	0.22	0.24	0.38	0.95	1.44
Timbuctoo	0.11	47.96	0.28	0.36	0.60	0.07	0.99	1.20
Morphological unit cross-sectional HG results								
Riffle	0.17	35.70	0.53	0.09	0.29	0.35	0.99	1.17
Pool	0.11	35.02	0.15	1.16	0.70	0.03	0.97	1.34
	Percent error = 100·(HG - HT)/HT							
100-m cross-sectional HG percent error								
Segment	-1.1	1.0	34	-28	-14	49		
Marysville	3.6	-3.0	36	-25	-12	53		
DPD	-0.7	2.2	11	-13	-8	23		
Timbuctoo	-1.8	1.9	44	-30	-12	50		
1-km cross-sectional HG percent error								
Segment	11	-2.2	48	-41	-25	93		
Marysville	-45	48	40	-19	-6.9	6.6		
DPD	39	-33	11	-23	-43	159		
Timbuctoo	-25	23	53	-33	-8.0	27		
Morphological unit cross-sectional HG percent error								
Riffle	-	-	-17	43	-11	0.6		
Pool	-	-	-21	-11	-4.9	29		

Table 4

(a) Average percent error magnitude (PEM) for each spatial scale and regression parameter; PEM is the absolute value of percent error values from Table 3 averaged among all regression parameter PEMs across each scale and then all scale PEMs for each regression parameter.
(b) PEMs averaged over only reach spatial scales (included 100-m and 1-km data) for each regression parameter

(a) All scales		(b) Reaches only	
Segment	29	b	19
Reach	27	a	19
MU	17	f	33
b	16	c	24
a	14	m	15
f	32	k	53
c	26		
m	14		
k	49		

Table 5
Percent error results comparing most representative HG cross section to HT benchmark

	Percent error			
Domain	b	f	m	Distance[a]
Segment[b]	-8.3	2.14	4.12	4.5
Marysville[b]	-15.15	-0.11	1.58	6.1
DPD[b]	-4.35	7.23	-1.86	4.2
Timbuctoo[b]	2.99	4.39	2.69	3.3
Riffle	-0.61	-7.68	-	7.7
Pool	3	1.48	-	3.3

[a] Distance formula derived from the Pythagorean theorem.

[b] Most representative among 100-m samples.

List of Figures

Fig. 1. A schematic that shows the complex array of considerations involved in generating at-a-station hydraulic geometry relationships. Few of these decisions are ever reported. See supplemental materials section 1.2 for detailed explanation.

Fig. 2. Location map of California showing the Yuba River catchment inset (top right) and the valley corridor of the lower Yuba River (bottom), with key locations shown. Boxes designate the extents of the three geomorphic reaches analysed.

Fig. 3. Log-log plots showing discharge-dependent HT and HG relations for the river segment (A,D,G), riffle MU (B,E,H), and pool MU (C,F,I). Rows represent hydraulic variables. Solid (near-census (NC) HT) and dashed (~ 100-m and 1-km spaced station derived HG) lines within each plot are the best fit power functions for a particular sample scheme. Minimum and maximum values are single station averages for a given flow (based on 100-m spaced stations for segment and one of 15 riffle and 14 pool stations). Near-census MU width is not displayed because it is constant with discharge.

Fig. 4. Same as in Fig. 3, but showing discharge-dependent HT and HG relations for Marysville (A,D,G), Daguere Point Dam (B,E,H), and Timbuctoo Bend (C,F,I) reaches.

Fig. 5. Ternary diagrams for each geomorphic reach (A,B,C) and one showing the relative locations of segment and reach HT and HG averages (D). Except for the last

UNCORRECTED FINAL MANUSCRIPT

diagram, points show the combination of *b*, *f*, and *m* for every cross section in that reach.

Fig. 6. A phase plot of *m* and *f* exponents from HT and HG analyses.

UNCORRECTED FINAL MANUSCRIPT

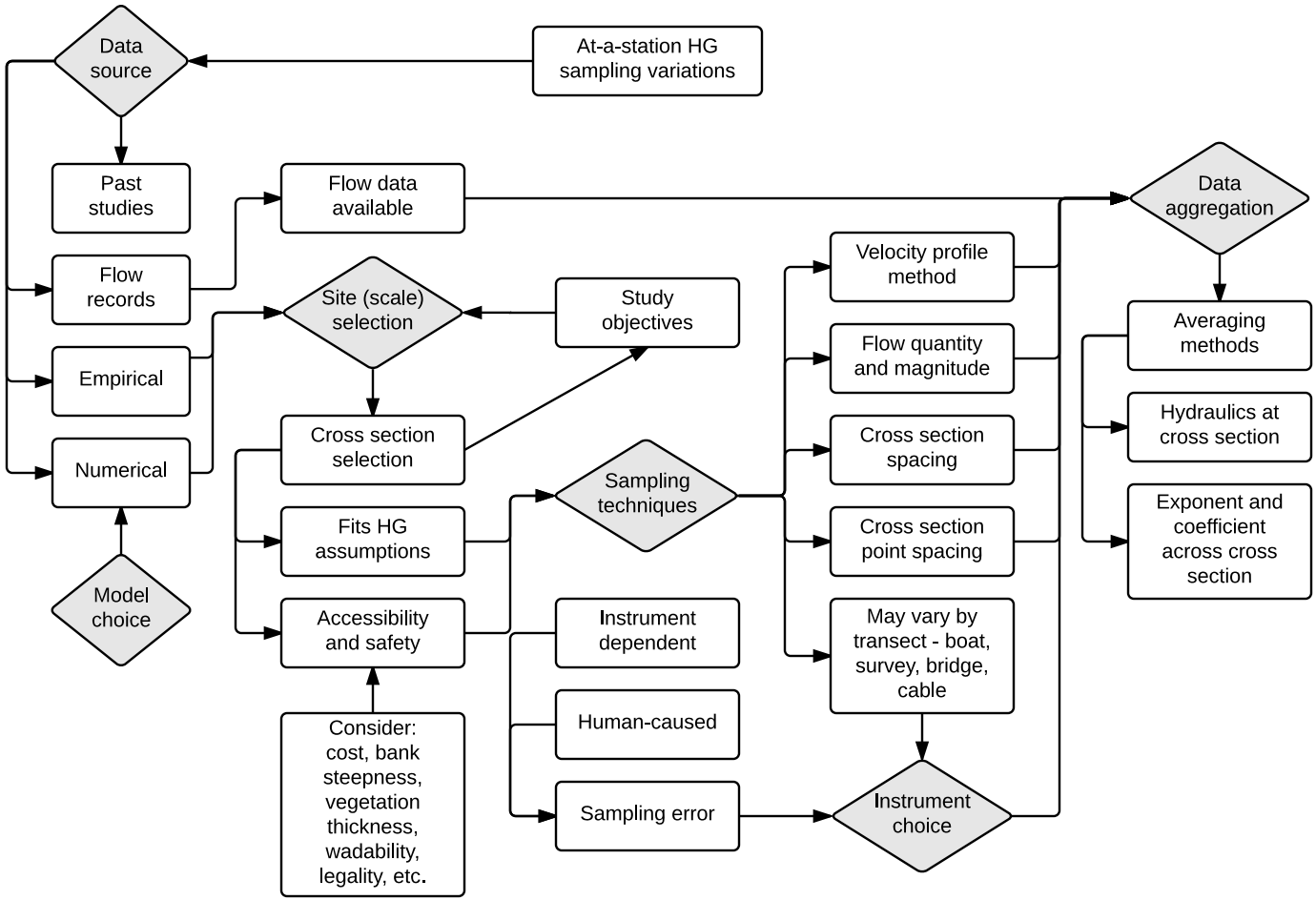
Data source
At-a-station HG sampling variations
Past studies
Flow records
Empirical
Numerical
Model choice
Flow data available
Site (scale) selection
Study objectives
Cross section selection
Fits HG assumptions
Accessibility and safety
Consider: cost, bank steepness, vegetation thickness, wadability, legality, etc.
Sampling techniques
Instrument dependent
Human-caused
Sampling error
Velocity profile method
Flow quantity and magnitude
Cross section spacing
Cross section point spacing
May vary by transect - boat, survey, bridge, cable
Instrument choice
Data aggregation
Averaging methods
Hydraulics at cross section
Exponent and coefficient across cross section

Figure 2

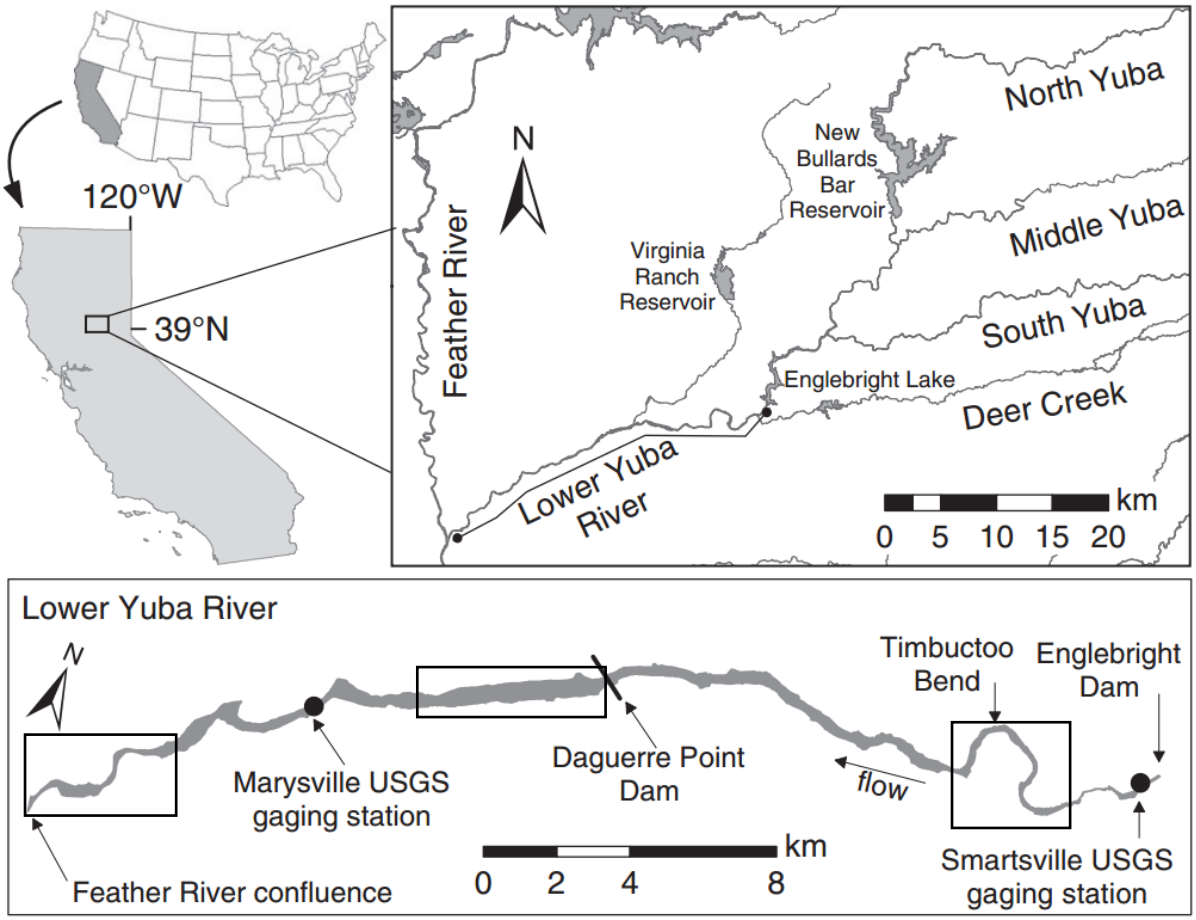
120°W
39°N
N
Feather River
New
Bullards
Bar
Reservoir
Virginia
Ranch
Reservoir
North Yuba
Middle Yuba
South Yuba
Englebright Lake
Deer Creek
Lower Yuba
River
km
0 5 10 15 20
Lower Yuba River
N
Timbuctoo
Bend
Englebright
Dam
Marysville USGS
gaging station
Daguerre Point
Dam
flow
Feather River confluence
km
0 2 4 8
Smartsville USGS
gaging station

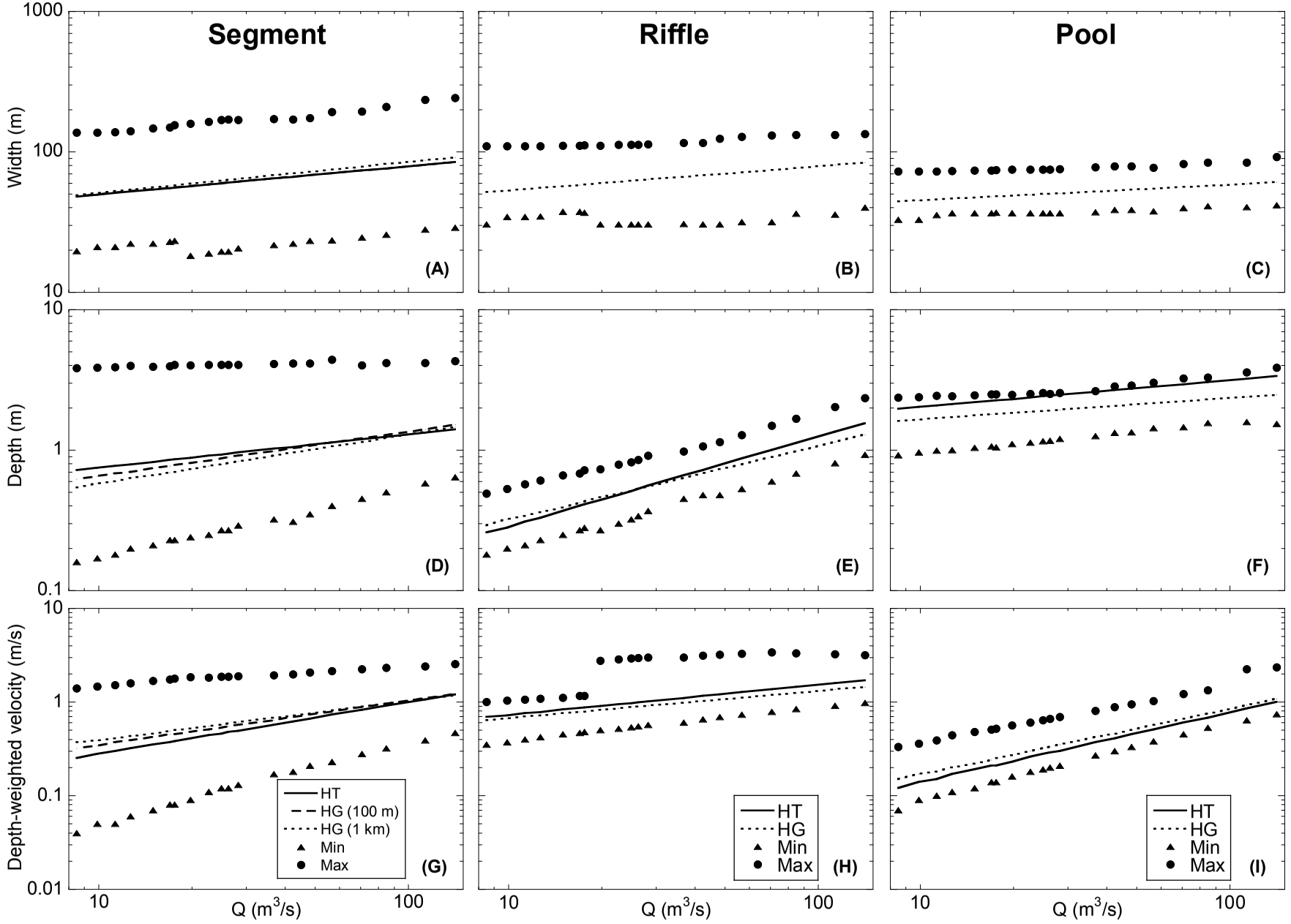
Segment
Riffle
Pool
Width (m)
Depth (m)
Depth-weighted velocity (m/s)
Q (m3/s)
1000
100
10
1
0.1
0.01
(A)
(B)
(C)
(D)
(E)
(F)
(G)
(H)
(I)
HT
HG (100 m)
HG (1 km)
HG
Min
Max

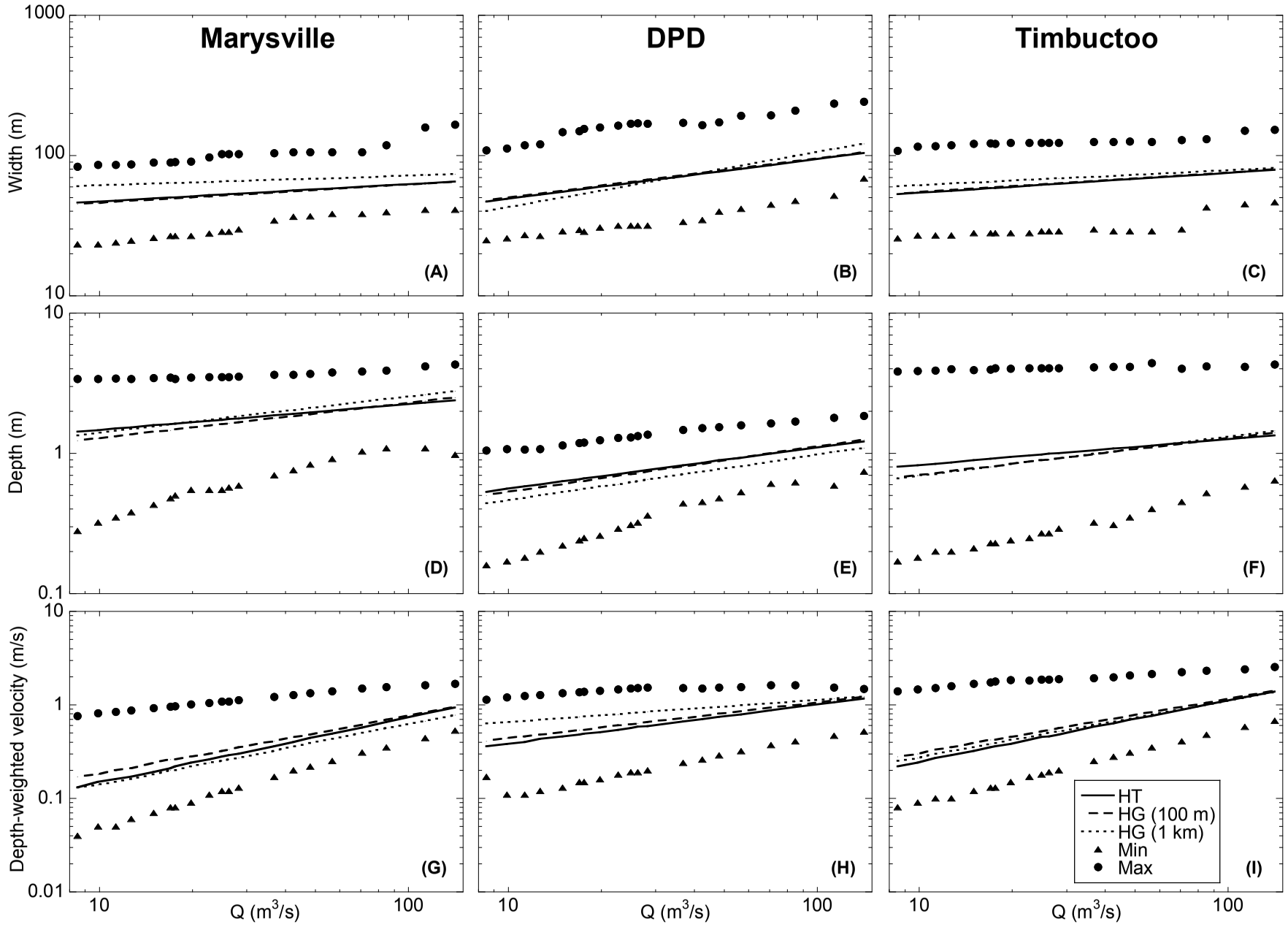
Marysville
DPD
Timbuctoo
Width (m)
Depth (m)
Depth-weighted velocity (m/s)
1000
100
10
1
0.1
0.01
(A)
(B)
(C)
(D)
(E)
(F)
(G)
(H)
(I)
Q (m3/s)
10
100
HT
HG (100 m)
HG (1 km)
Min
Max

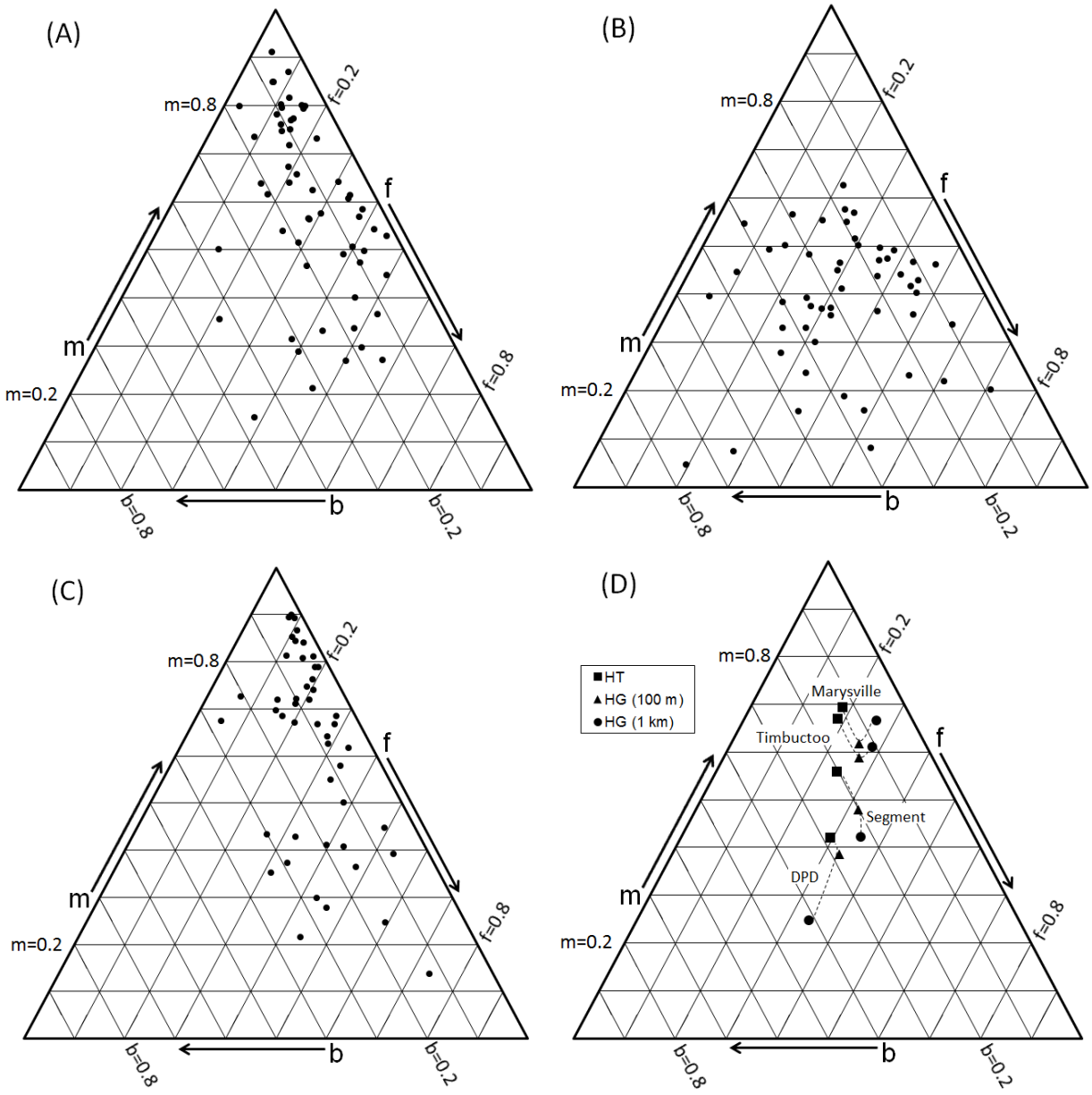
(A)
m=0.8
f=0.2
f
m
m=0.2
f=0.8
b=0.8
b
b=0.2
(B)
m=0.8
f=0.2
f
m
m=0.2
f=0.8
b=0.8
b
b=0.2
(C)
m=0.8
f=0.2
f
m
m=0.2
f=0.8
b=0.8
b
b=0.2
(D)
HT
HG (100 m)
HG (1 km)
Marysville
Timbuctoo
Segment
DPD
m=0.8
f=0.2
f
m
m=0.2
f=0.8
b=0.8
b
b=0.2

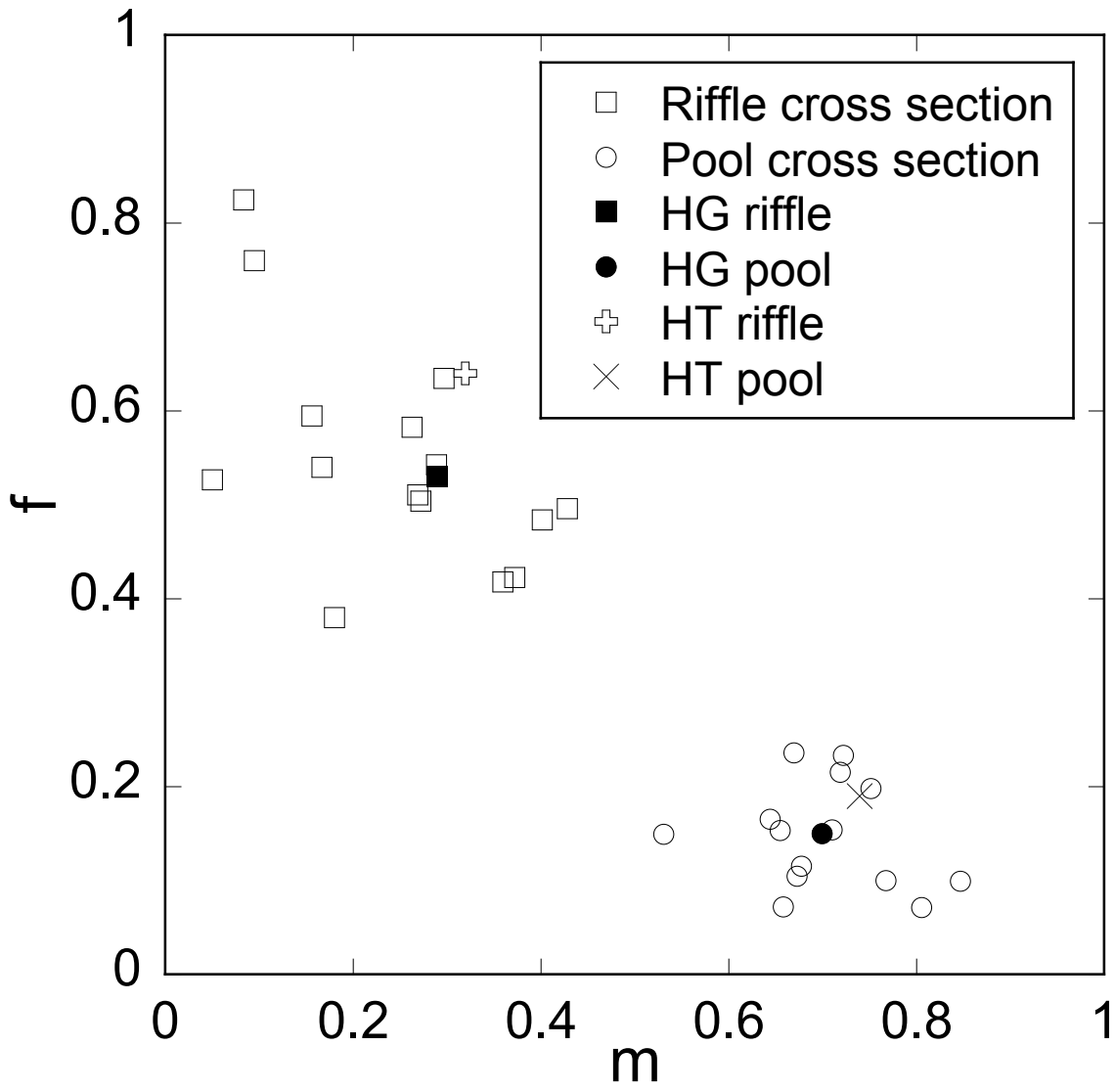
Riffle cross section
Pool cross section
HG riffle
HG pool
HT riffle
HT pool
f
m
0
0.2
0.4
0.6
0.8
1

Supplemental materials

1 Introduction Supplements

1.1 Near-census river science

Many surveying methods are available to collect data at a resolution of 1 pt/m^2. In the 1990s and 2000s, real-time kinematic global positioning system and robotic total stationing were the dominant technologies for meter-scale mapping (e.g., Brasington et al., 2000; Sawyer et al., 2010). Through the 2000s airborne LiDAR mapping of subaerial land at meter-scale resolution increased and is now widespread. As of 2015, it is common for a single airborne LiDAR pass to return ~9 pts/m^2 in open to lightly vegetated terrain, with overlapping passes having one to two orders of magnitude higher point density. Whole countries have been mapped at meter to submeter resolution. As of April 2015, the website OpenTopography publicly provided airborne LiDAR data for 179,153 km^2 of land. Airbone LiDAR data for subaqueous terrain is emerging, but is behind that for subaerial terrain. Nevertheless, it is just a question of time until meter-scale topography for the whole world is available, so it is very much time to work out the basic and applied science that can make use of this data.

The term ‘near-census’ is used herein to refer to comprehensive, spatially explicit, process-based approaches using the 1-m scale as the basic building block for investigating rivers in light of the emerging abundance of meter-scale topographic datasets without the confounding problems associated with sampling. The concept of a ‘near-census’ implies that meter-scale data represents variables in great detail that approaches the population of conditions, but that there remains a finer level of detail in the domain of continuum mechanics that eventually will be resolved with further technological developments. For example, our experience is that terrestrial laser scanning (TLS) produces DEMs with millimeter to decimeter resolution, which is far beyond what geomorphology and hydraulics are prepared to cope with at

this stage of science. However, that potential means that we cannot use the tern “census” for meter-scale data, and thus we use “near-census”.

Near-census mapping and numerical modeling require that topographic data collection is done fully and mindfully so that terrain complexity at the 1-m scale is captured and represented in subsequent 2D or 3D hydrodynamic and/or morphodynamic simulations and analyses. Near-census river science aims to represent key parameters of multiple spatial scales of a river at a high enough resolution so that uncertain interpolations and extrapolations are minimized. It enables spatial averaging of output hydraulics comprehensively at multiple spatial scales while taking into account local variations. Using near-census data, one can generate ‘hydraulic topography’ relations at any spatial scale down to the 1-m resolution threshold.

1.2 Uncertainties in at-a-station hydraulic geometry

The point of this section is not to criticize past researchers and studies, but to firmly establish the potential value in re-envisioning this important tool with new technology that eliminates many of the subjective, unstated decisions made in HG analysis. Sampling, as a paradigm for applying the scientific method, is inherently biased and fraught with confounding complexities relating to study-specific choices, many of which may go unexplained or unsupported in the literature for a host of reasons (Figure 1). Field-based surveys are typically constrained by accessibility, time, and financial resources. Dense vegetation, steep terrain, rapids, remoteness, and private property may limit where it is safe or physically possible to gather data. Flood flows are infrequent and dangerous to survey, and thus tend to be excluded from analysis. Sometimes post-flood debris-line elevations are used to reconstruct high flow stages, with some uncertainty. Other uncertainties arise from data types or sources, cross section placement, the number of measurements per transect, and methods for aggregating and averaging the data. While some researchers collect their own cross-sectional field data and a few simulate that using hydraulic models, a majority of HG researchers use historic discharge

52 records as their primary dataset (Leopold and Maddock, 1953; Emmett, 1975). Detailed
53 hydrographer notes and rating curves are frequently used to generate HG relations (Emmett,
54 1975; Turnipseed and Sauer, 2010). It may be problematic that HG relations are so often
55 derived from stable cross sections specifically chosen to calculate discharge (Park, 1977). In
56 addition, Ponton (1972) pointed out that slightly different gaging stations may be used at
57 different flows, particularly if cableway and wading measurements are taken at the same
58 location.

59 When sampling a cross section for discharge (and later using that data for an HG study),
60 some basic assumptions are that the channel is in a state of quasi-equilibrium with respect to
61 sediment transport and that flows are uniform and steady. In reality, naturally formed streams
62 are rarely uniform. Another fundamental condition is that channel cross section is stable and
63 persistent through time (Figure 1). Other selection guidelines include that the channel be single-
64 threaded and relatively straight with parallel banks. While standardized methods stress the
65 importance of site selection, little guidance is offered when ideal sites are not present, as
66 demonstrated in a recent U.S. Geological Survey manual on discharge measurements: “It is
67 usually not possible to attain all of these conditions, but site selection cannot be understated as
68 a critical part of a discharge measurement. Select the best possible reach using these criteria
69 and then select a cross section” (Turnipseed and Sauer, 2010). To further challenge the HG
70 scientist, ideal HG station sites span natural, self-formed rivers free from man-made
71 infrastructure such as flumes, bridges, or hardened banks.

72 It has been acknowledged that differences in gage versus field data (Park, 1977),
73 measurement error, and station location choice (Stewardson, 2005) affect traditional HG results.
74 King et al. (2004) provided an observation that captures some of this ambiguity: “One consistent
75 set of methods does not necessarily apply to all of the study sites or to all of the data for a given
76 study site. This is due to reliance on previously collected information by different agencies for a
77 variety of purposes…” Known sampling bias is another limitation that should be reported. For

example, considerable variability in hydraulic exponents among Idaho streams was in part explained by data collection techniques such as sampling at flow-constricting bridges and by preferential surveying of wider, more wade-able sections at high flows (Emmett, 1975).

Considerable effort has been focused on understanding at-a-station HG similarities between different rivers instead of differences within one river network. Park (1977) made a comparison of global studies by climate type and concluded that accounting for the variability in HG relationships is more important than grouping them by shared physiographic characteristics. Given the narrow range of possible HG exponent values, perhaps arriving at numbers consistent with previous literature limits the ability to communicate a range of HG relationships seen within a system.

Some uncertainties were addressed by Stewardson (2005), where it was suggested that hydraulics measured in the field are better suited to develop HG relations than modeled hydraulics, but no transect placement advice or explanations were provided. It is hard to justify cross study comparison when sample methodology is so variable- though it is done out of necessity regardless of its technical unsoundness.

2 Study Site Supplements

None.

3 Methods Supplements

3.1 Physical data information

Field data collection efforts were explicitly intended to characterize geomorphic, hydrologic, and hydraulic attributes of the LYR at roughly meter-scale resolution in support of a near-census approach to river assessment, including 2D hydrodynamic modeling. The types of data collected included topography and bathymetry (Pasternack, 2009; White et al., 2010;

Carley et al., 2012) as well as hydraulic data: water surface elevation, depth, velocity magnitude, and velocity direction (Barker, 2011; Pasternack et al., 2014). Details about spatial coverage, resolution, and accuracy for the digital elevation model (DEM) used in this study are provided below.

Topographic data came from airborne LiDAR scanning (excluding Timbuctoo Bend) at flows ~ 10–16% of bankfull discharge plus thorough in-water mapping using total stations and RTK GPSs as well as boat-based bathymetry mapping with a single-beam echosounder coupled to an RTK GPS and professional hydrographic software. Basic information describing topographic and bathymetric field data in the Yuba River downstream of Englebright Dam are reported in the box below.

Attribute	Description
Aerial extent	Entire river, except the Narrows Reach
Years of data collection	Englebright Dam Reach (EDR) was mapped in 2005 and 2007 and Timbuctoo Bend Reach (TBR) was mapped in June–December 2006. From highway 20 down, most bathymetry was mapped in late August to early September 2008, with some high-flow data collection in March and May 2009 as well as small additional near-bank and near-DPD gaps mapped in November 2009. Ground-based topographic surveys were done in November 2008 and November 2009. Lidar of the terrestrial river corridor was flown on September 21, 2008.
Bathymetric Resolution	EDR: Within the 880 cfs inundation area, points were collected along longitudinal lines, cross-sections, and on ~5'x5' grids, yielding an average grid point spacing of one point every 4.5 ft. (54.3 pts/100m^2). TBR: Within the 880 cfs inundation area, points were collected along longitudinal lines, cross-sections, and on ~10'x10' grids, yielding an average grid point spacing of one point every 6.2 ft. (28 pts/100m^2). All else: Within the 880 cfs inundation area, points were collected along longitudinal lines, some cross-sections, and some localized grids. The average grid point spacing is one point every 4.2 ft. (59.8 pts/100m^2).
Topographic Resolution	EDR: Outside the 880 cfs inundation area, points were collected with a combination of grid-based ground-based reflectorless laser scanning of canyon walls and total station surveys of accessible ground, yielding an average grid point spacing of one point every 5.9 ft. (31.3 pts/100m^2). TBR: Outside the 880 cfs inundation area, points were collected on a grid, yielding an average grid point spacing of one point every 9.7 ft. (11.4 pts/100m^2).

	All else: Outside the 880 cfs inundation area, points were mostly collected with lidar, yielding an average grid point spacing of one point every 1.4 ft. (554 pts/100m^2).
Bathymetric Accuracy	EDR: comparison of overlapping echosounder and total station survey points yielded observed differences of 0.2-0.3'. TBR: comparison of overlapping echosounder and total station survey points yielded observed differences of 0.2-0.3'. All else: comparison of overlapping echosounder and total station survey points at one site yielded observed differences of 50% within 0.5', 75% within 0.6', and 94% within 1'. Comparison of boat-based water edge shots versus RTK GPS surveyed water's edge shots yielded observed differences of 75% within 0.1', 91% within 0.2', and 99% within 0.5'.
Topographic Accuracy	EDR: regular total station control point checks yielded accuracies of 0.03-0.06'. TBR: regular total station control point checks yielded accuracies of 0.03-0.06'. All else: compared against 8,769 ground-based RTK GPS observations of elevation along flat surfaces, 54% of LIDAR points were within 0.1' , 86% were within 0.2', and virtually all of the data were within 0.5'. Regular total station control point checks yielded accuracies of 0.03-0.06'. RTK GPS observations had vertical precisions of 0.06'. Comparison of lidar water edge points versus the same for RTK GPS yielded observed differences of 30% within 0.1', 57% within 0.2', and 92% within 0.5'.

114

115 *3.2 2D hydrodynamic modeling details*

116 The surface-water modeling system (SMS; Aquaveo, LLC, Provo, UT) user interface and
117 sedimentation and river hydraulics–two-dimensional algorithm (Lai, 2008) were used to produce
118 these 2D hydrodynamic models of the LYR with internodal mesh spacing of 0.91–1.5 m
119 according to the procedures of Pasternack (2011). SRH-2D is a 2D finite-volume model that
120 solves the Saint Venant equations for depth and velocity at each computational node, and
121 supports a hybrid structured-unstructured mesh that can use quadrilateral and triangular
122 elements of any size, thus allowing for mesh detail comparable to finite-element models. A
123 notable aspect of the modeling was the use of spatially distributed and stage-dependent
124 vegetated boundary roughness (Katul et al., 2002; Casas et al., 2010). Model simulations were
125 comprehensively validated for flows ranging over an order of magnitude of discharge (0.1 to 1.0
126 times bankfull) using three approaches: (i) traditional cross-sectional validation methods, (ii)

127 comparison of LiDAR-derived water surface returns against modeled water surface elevations,
128 and (iii) Lagrangian particle tracking with RTK GPS to assess the velocity vectors. Model set-up
129 and performance details are reported in the box below:
130

Attribute	Description
Model domains	For the whole river, there were 5 modeling reaches to make the computational process more efficient. They are given the abbreviations, EDR, TBR, HR, DGR, and FR below. For maps and details about them, see (Pasternack et al., 2014)
Computational Mesh Resolution	EDR: 3' internodal spacing for all Q TBR: For Q<5,000 cfs, 3' internodal spacing. As flow goes overbank, cell size increases to 6'. For flows >21,100 cfs, different mesh has 10' internodal spacing. HR: For flows 0-1300 cfs, 3' internodal spacing. For flows 1300-7500 cfs, 5' internodal spacing. For flows >10,000, 10' internodal spacing. DGR: For flows 0-1300 cfs, 5' internodal spacing. For flows 1300-7500 cfs, 5' internodal spacing. For flows >10,000, 10' internodal spacing. FR: For flows 0-1300 cfs, 5' internodal spacing. For flows 1300-7500 cfs, 5' internodal spacing. For flows >10,000, 10' internodal spacing.
Discharge Range of Model	EDR was 700 to 110,400 cfs; all else was 300 to 110,400 cfs
Downstream WSE data/model source	EDR: Some WSE observations combined with slope-based translation of the Smartville gage WSE data to the end of the reach. TBR: Direct observation of WSE at a limited number of flows <~12,000 cfs. For higher flows the downstream WSE was taken as the upstream WSE from the HR model at that flow. HR: Continuous direct observation of WSE at flows <~22,000 cfs. For higher flows the downstream WSE was taken as the upstream WSE from the HR model at that flow. DGR: Reach ends exactly at Marysville gaging station, so the WSE data is of the highest quality and abundance. Continuous WSE data for all flows ~500 - 110,400 cfs. FR: Continuous direct observation of WSE at flows <~22,000 cfs. For higher flows the downstream WSE was set to yield an upstream WSE equal to that at the Marysville gage.
River roughness specification	Because the scientific literature reports no consistent variation of Manning's n as a function of stage-dependent

	relative roughness or the whole wetted area of a river (i.e., roughness/depth), a constant value was used for all unvegetated sediment as follows: 0.032 for EDR (a deeper bedrock canyon), 0.03 for TBR (based on preliminary testing in 2008-2009), and 0.04 for the rest of the LYR (based on validation testing of 0.03, 0.035, 0.04, 0.045, and 0.05 as possible options). For vegetated terrain, the Casas et al. (2010) algorithm was used to obtain a spatially distributed, flow-dependent surface roughness for each model cell on the basis of the ratio of local canopy height to flow depth.
Eddy viscosity specification	Parabolic turbulence closure with an eddy velocity that scales with depth, shear velocity, and a coefficient (e_0) that can be selected between ~0.05 to 0.8 based on expert knowledge and local data indicators. Q<10,000 cfs: e_0 = 0.6 Q≥10,000 cfs: e_0 = 0.1
Hydraulic Validation Range	Point observations of WSE were primarily collected at 880 cfs, with some observations during higher flows, but not systematically analyzed. Velocity observations were collected for flows ranging from 530-5,010 cfs. Cross-sectional validation data collected at 800 cfs above DPD and 540 cfs below DPD.
Model mass conservation (Calculated vs Given Q)	0.001 to 1.98 %
WSE prediction accuracy	At 880 cfs there are 197 observations. Mean raw deviation is -0.006'. 27% of deviations within 0.1', 49% of deviations within 0.25', 70% within 0.5', 94% within 1'. These results are better than the inherent uncertainty in LiDAR obtained topographic and water surface elevations.
Depth prediction accuracy	From cross-sectional surveys, predicted vs observed depths yielded a correlation (r) of 0.81.
Velocity magnitude prediction accuracy	5780 observations yielding a scatter plot correlation (r) of 0.887. Median error of 16%. Percent error metrics include all velocities (including V <3ft/s, which tends to have high error percents) yielding a rigorous standard of reporting.
Velocity direction prediction accuracy	5780 observations yielding a scatter plot correlation (r) of 0.892. Median error of 4%. Mean error of 6%. 61% of deviations within 5 deg and 86% of deviations within 10 deg.

131

132 Using the workflow of Pasternack (2011), SRH-2D model outputs were processed to
133 produce rasters of depth and velocity within the wetted area for each discharge. The first task
134 involved creating the wetted area polygon for each discharge. To do this, depth results were first
135 converted to triangular irregular networks (TIN) and then to a series of 0.9144-m hydraulic raster

files. Depth cells greater than zero were used to create a wetted area boundary applied to all subsequent hydraulic rasters. Next, the SRH-2D hydraulic outputs for depth and depth-averaged velocity were converted from point to TIN to raster files within ArcGIS 10.1 staying within the wetted area for each discharge. The complete dataset was a series of 0.9144-m resolution hydraulics rasters derived from SRH-2D hydrodynamic flow simulations at the following discharges: 8.5, 9.9, 11.3, 12.7, 15.0, 17.0, 17.6, 19.8, 22.7, 24.9, 26.3, 28.3, 36.8, 42.5, 48.1, 56.6, 70.8, 85.0, 113.3, and 141.6 m^3/s.

Despite best efforts with modern technology and scientific methods, the 2D models used in this study have uncertainties and errors. Previously it has been reported that 2D models tend to underrepresent the range of hydraulic heterogeneity that likely exists due to insufficient topographic detail and overly efficient lateral transfer of momentum (Pasternack et al., 2004; MacWilliams et al., 2006). For this study those deficiencies result in a conservative outcome, such that real differences between true HT and sampled HG would be even greater than what would is revealed herein. Overall, this study involves model-based scientific exploration with every effort made to match reality at near-census resolution over tens of km of river length given current technology, but recognizing that current models do have uncertainties.

3.3 Hydraulic model results analysis

Post-2D model workflow details and decisions from this study are documented below to produce transparent and reproducible science. In both near-census and cross-sectional cases, a preliminary goal was to generate power equations that represented the hydraulics as a function of discharge at each scale: segment, reach, and morphological unit. Once power functions were fit to the average hydraulic variable data for each combination of methodology and spatial scale, the associated coefficients and exponents were extracted. The notes below focus first on near-census, then on cross-sectional methods, and work through each combination of hydraulic type and spatial scale.

3.4 Hydraulic topography workflow

3.4.1 Hydraulic topography depth

Depth was the simplest hydraulic variable to calculate. In ArcGIS, the Spatial Analyst tool, 'Zone Statistics as Table', was used to calculate the arithmetic average of all raster cell values contained within a specified spatial extent (i.e. segment, reach, or MU scale) for each modeled discharge. The wetted area polygon or MU shapefile was input as the 'Feature Zone Data' and depth raster as the 'Input Value Raster.' The 'Ignore NoData in Calculations' box was checked. The mean, standard deviation, and maximum values were transferred to an Excel spreadsheet where the data could be organized.

3.4.2 Hydraulic topography velocity

Determining near-census average velocity magnitude was not as straightforward because it could be considered in 2 or 3 dimensions. SRH-2D velocity output points and subsequently extrapolated TIN surfaces and raster cells represented depth-averaged velocities. To spatially average those velocity pixels would produce an average depth-averaged velocity for some spatial scale, with relatively deep and shallow pixels receiving equal weight. This is fine if the goal is to characterize average plan view velocity. However, if one seeks to represent the average velocity at any point in the 3-dimensional space of the flowing river, then relative depths must be considered in the calculation.

We decided on an averaging method that weighted velocities based on the local cell depth (see 'Cross section sampling workflow', step #5). This is analogous to the convention of weighting velocity by conveyance to determine cross-sectional average velocity: divide total discharge by the cross-sectional area instead of averaging depth-averaged velocities along the cross section. To obtain near-census depth-weighted velocity, we weighted every individual

depth-averaged velocity pixel by the corresponding depth before applying the zonal statistics spatial averaging tool. In other words, each depth-averaged velocity cell value was multiplied by the ratio of the corresponding depth pixel to average depth for the spatial scale being considered. This created a completely new raster whose cells were then averaged over the associated spatial scale using the zone statistics method as described above.

The effects of depth-weighting near-census velocity pixels are shown for each spatial scale in the following plots:

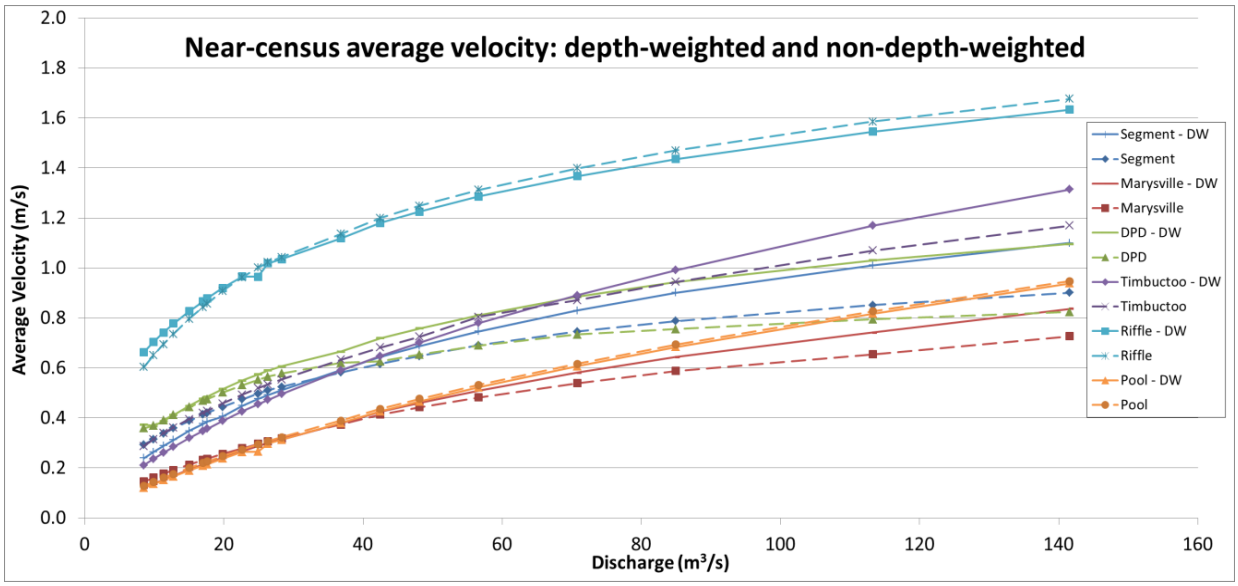

Appendix 1. A plot showing the effects of depth weighting the full set of near-census velocity data. 'DW' signifies 'depth weighted'. Lack of 'DW' refers to the non-DW data, which were the arithmetic mean of depth-averaged velocity cells over that spatial scale.

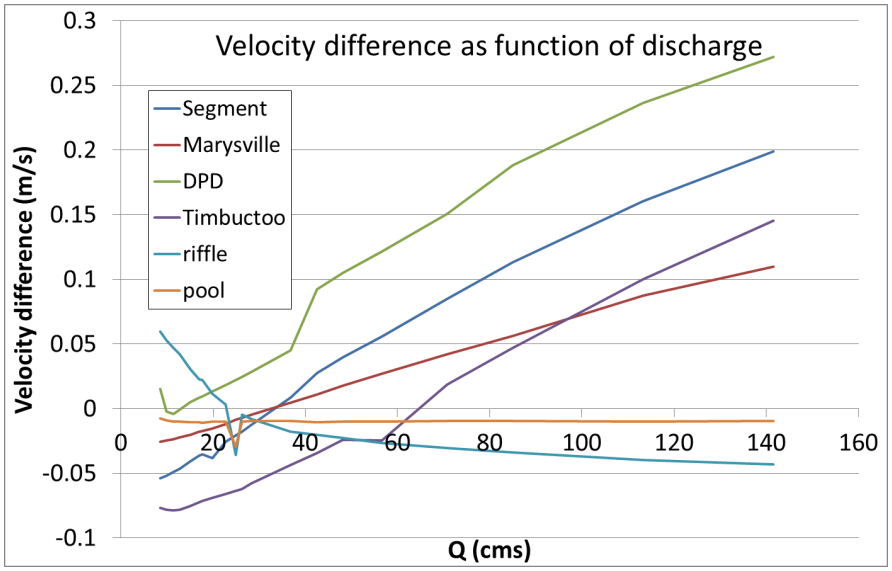

Appendix 2. A plot of velocity difference between DW and non-DW for each spatial scale.

3.4.3 Hydraulic topography top width

Near-census widths for segment and reach scales were derived from station lines spaced every 6.1 m along the LYR. Stations were oriented perpendicular to the LYR valley centerline and locked in place for all flows. The valley centerline was created by hand using 'Editor' in ArcGIS. To create station lines, the ArcGIS add-on tool pack 'ET GeoWizard' was opened and the function 'Points along a Polyline' was used to create a set of points of a user-determined spacing along the centerline. Next the 'Create Station Lines' tool was used to create lines at the previous polyline points that radiate out perpendicularly to a user-determined distance (long enough to span the wetted area polygons at bankfull discharge). This produced the master station line file that was then clipped to 20 wetted area polygons corresponding to 20 different flows up to bankfull. Next, a field was added to the attributes table and lengths of each station line were calculated. This data was exported to Excel to be organized by unique station number and associated flow. The geometric mean of station lengths for each discharge was calculated for both segment and reach spatial scales. The geometric mean of a station-averaged hydraulic dataset ($a_1, a_2, a_3 \ldots a_n$) is given by:

$$a_G = (\prod_{i=1}^{n} a_i)^{\frac{1}{n}} = \sqrt[n]{a_1 a_2 \dots a_n}$$

where a_G is the geometric mean of that hydraulic variable, and n is the number of cross sections in the data domain.

Near-census MUs were defined as being an expression of the underlying bedform and independent of discharge. Consequently, near-census MU widths were not calculated.

3.5 Hydraulic geometry analysis

Transect-derived reach HG could be determined using three types of averaging. The first is by averaging all sampled points from each cross section that comprise that reach for each flow, and generating a discharge-relationship. The method used in this study, was to first calculate cross section averages then weight each section in the final averaging by spacing, equally in this case. Another possible, but not advisable method, would be to generate HG curves for every cross section first, and then average the resulting exponents and coefficients obtained from regression.

Station lines used to simulate cross-sectional sampling for segment and reach scales were a 97.54 m spaced subset of those spaced 6.1 m used for near-census width determination. The stations were spot checked for perpendicularity to centerline and banks at low and bankfull flows. An additional subset was created with lines spaced every 975.36 m.

Several decisions were made to minimize factors contributing to methodological comparison uncertainty. For example, only a single power function was fit to the hydraulic data for each sampling approach. The same twenty discharges up to bankfull were sampled by each method to ensure equal representation when log-linear regressions were applied. A uniformly spaced cross-sectional sampling strategy prevented overlap and enabled equal weighting for aggregation at larger spatial scales.

242 Also, the same type of depth weighting of velocity data was applied in HT and HG
243 analyses. Systematic sampling of the 2D model dataset along cross sections provided a
244 single consistent source of many depth and velocity values beyond what has been
245 reported in the past. Even though 2D models can underrepresent the spatial
246 heterogeneity of turbulent, shallow rivers, there is presently no method of field sampling
247 or remotely observing near-census hydraulics over tens of kilometers. Thus, the
248 limitations of 2D modeling are outweighed by the experimental value of having all
249 sampling techniques utilize the same hydraulics population, which yields a fair and
250 meaningful comparison.

251 A protocol was developed on how to select riffle and pool MUs to sample along the LYR
252 segment. The MU pixel threshold of with contiguous area greater than 92.8 m^2 or ≥ 111 pixels
253 were based on previous work done on the LYR (Wyrick and Pasternack, 2012). Units that met
254 this size condition were randomly selected using Excel's 'RANDBETWEEN' function.

255

256 *3.6 Cross section sampling workflow*

257 1. Create 30 equally spaced station points along each cross section using the 'Construct
258 Points' Editing tool in ArcGIS. This was done one station at a time and for every
259 discharge since the wetted width changes with flow. Thirty sample points per cross
260 section was selected as it is the USGS survey protocol gold standard.
261 2. Use Spatial Analyst's 'Extract Values to Points' tool to transfer depth and velocity raster
262 data to the set of points for each discharge.
263 3. Export all point file attributes tables to Excel for subsequent calculations. It was
264 discovered that some points located at station line endpoints had a depth and/or velocity
265 value of -9999, which is not possible. Values were amended to 0.01 m or 0.01 m/s to
266 better represent near-bank hydraulics and so that averages would be positive.

4. Calculate average depth at each station for each discharge using a simple arithmetic mean. Ie. Average the thirty depth measurements along each cross section for all flows. Over 200,000 sample points needed to be averaged in specific combinations given the thirty sample points that comprise each of the 354 stations (spaced at 97.54 m along the segment) for 20 modeled discharges. An array formula was used to reference the corresponding station number and discharge for calculations of this nature.
5. Cross-sectional velocity magnitude values were calculated. Velocity was weighted by the conveyance of the region below each sample point. The procedure was to multiply each depth-averaged velocity value by the ratio of the corresponding depth to average cross-sectional depth, and then arithmetically average those values. The station-averaged depth for a given station is constant for each flow, so it can be pulled outside of the summation sign. The equation used to calculate average depth-weighted station velocity magnitude ($\overline{V}_{XS}$) was:

$$\overline{V}_{XS} = \frac{1}{30\overline{D}_{XS}} \sum_{i=1}^{30} V_{p_i} D_{p_i}$$

where $\overline{D}_{XS}$ is a the average cross-sectional depth, V_{p_i} represents the depth-averaged velocities at the thirty sample points along the cross section, and D_{p_i} represents the depth values at the same thirty points. This equation was applied to each cross section for all twenty flows in order to develop the HG relations.
6. Gather the station identification numbers and associated widths for each discharge.
7. Calculate the geometric mean of station-averaged hydraulics for each discharge and spatial scale combination to generate the data points to be fit with a power function. For example, to obtain the DPD reach depth HG relationship, plug in average cross section depth values from along DPD into the geometric mean equation for a single flow, repeat for remaining flows, plot as a function of discharge, and fit a power function to the data.

8. Lastly, a MATLAB script was used to efficiently fit power functions and generate associated coefficients, exponents, and R^2 values for near-census, station-averaged, and individual station hydraulic data. The MATLAB code below may need to be tweaked depending on the input file format.

```
clc
clear all
close all

%MATLAB Script: April 6th, 2014

%Input hydraulics data from multiple Excel spreadsheets
stations = xlsread('Stations');
depth = xlsread('Depth_data');
velocity = xlsread('Velocity_data');
width = xlsread('Width_data');
discharge = xlsread('Discharge');
discharge_constrained = discharge(8:20);

%DEPTH analysis
%Loop through all 383 cross sections along the Lower Yuba River (LYR) for i = 1:383;
        if i > 368 %XS in this portion of the LYR are missing hydraulics data at lower Q
                row = depth(i,8:20);
                p = polyfit(log(discharge_constrained),log(row),1); %Linear best fit on loglog data
                = power fit
                r = corrcoef(log(discharge_constrained),log(row));
        else
                row = depth(i,:);
                p = polyfit(log(discharge),log(row),1);
                r = corrcoef(log(discharge),log(row));
        end
                depth_result(i,1) = stations(i); %Create results table
                depth_result(i,2) = p(1); %Exponent of fitted power function
                depth_result(i,3) = exp(p(2)); %Coeff of fitted power function
                depth_result(i,4) = r(1,2)^2; %R^squared value
end
```

Supplemental References

Brasington, J., Rumsby, B.T., McVey, R.A., 2000. Monitoring and modeling morphological change in a braided gravel-bed river using high-resolution GPS-based survey. Earth Surface Processes and Landforms 25(9), 973-990.

Casas, A., Lane, S.N., Yu, D., Benito, G., 2010. A method for parameterising roughness and topographic sub-grid scale effects in hydraulic modelling from LiDAR data. Hydrology and Earth System Sciiences. 14(8), pp.1567-1579.

Emmett, W.W., 1975. The channels and waters of the upper Salmon River area, Idaho. Geological Survey Professional Paper 870-A Washington, D.C.

Katul, G., Wiberg, P., Albertson, J., Hornberger, G., 2002. A mixing layer theory for flow resistance in shallow streams. Water Resources Research, 38(11), 8.

King, J.G., Emmett, W.W., Whiting, P.J., Kenworthy, R.P., Barry, J.J., 2004. Sediment transport data and related information for selected coarse-bed streams and rivers in Idaho. General Technical Report RMRS-GTR-131, p. 4.

Lai, Y.G., 2008. SRH-2D version 2: Theory and User's Manual. In: B.o.R. U.S. Department of Interior (Ed.), Sedimentation and river hydraulics – two-dimensional river flow modeling, Denver, CO.

Park, C.C., 1977. World-wide variations in hydraulic geometry exponents of stream channels — analysis and some observations. Journal of Hydrology, 33(1-2), 133-146.

Pasternack, G.B., 2011. 2D Modeling and Ecohydraulic Analysis. Createspace, Seatle, WA.

Pasternack, G.B., Tu, D., Wyrick, J.R., 2014. Chinook adult spawning physical habitat of the lower Yuba River, Prepared for the Yuba Accord River Management Team. University of California, Davis, CA.

Ponton, J.R., 1972. Hydraulic geometry of Green and Birkenhead rivers: Southwestern Coast Mountains, British Columbia, University of British Columbia.

Sawyer, A.M., Pasternack, G.B., Moir, H.J., Fulton, A.A., 2010. Riffle-pool maintenance and flow convergence routing observed on a large gravel-bed river. Geomorphology, 114(3), 143-160.

Stewardson, M.J., 2005. Hydraulic geometry of stream reaches. Journal of Hydrology, 306(1-4), 97-111.

Turnipseed, P.D., Sauer, V.B., 2010. Discharge Measurements and Gaging Stations: U.S. Geological Survey Techniques and Methods book 3. Reston, VA.

Wyrick, J.R., Pasternack, G.B., 2012. Landforms of the Lower Yuba River, Prepared for the Lower Yuba River Accord Planning Team. University of California, Davis, CA.

Wyrick, J.R., Pasternack, G.B., 2014. Geospatial organization of fluvial landforms in a gravel–cobble river: beyond the riffle–pool couplet. Geomorphology, 213, 48-65.